Taylor & Francis
Taylor & Francis Group

RESEARCH PAPER

🔓 OPEN ACCESS   Check for updates

HIV-1 Nef counteracts autophagy restriction by enhancing the association between BECN1 and its inhibitor BCL2 in a PRKN-dependent manner

Sergio Castro-Gonzalez[a], Yuhang Shi[a]*, Marta Colomer-Lluch[b]*, Ying Song[c], Kaitlyn Mowery[a], Sharilyn Almodovar[d], Anju Bansal[e], Frank Kirchhoff[f], Konstantin Sparrer [f], Chengyu Liang[c], and Ruth Serra-Moreno[a]

[a]Biological Sciences, College of Arts and Sciences, Texas Tech University, Lubbock, TX, USA; [b]IrsiCaixa AIDS Research Institute, Germans Trias i Pujol Research Institute, Badalona, Spain; [c]Molecular Microbiology and Immunology, Keck School of Medicine, University of Southern California, Los Angeles, CA, USA; [d]Immunology and Molecular Microbiology, Texas Tech Health Sciences Center, Lubbock, TX, USA; [e]Medicine, Infectious Diseases, University of Alabama at Birmingham, Birmingham, AL, USA; [f]Institute of Molecular Virology, University of Ulm, Ulm, Germany

ABSTRACT

Macroautophagy/autophagy is an auto-digestive pro-survival pathway activated in response to stress to target cargo for lysosomal degradation. In recent years, autophagy has become prominent as an innate antiviral defense mechanism through multiple processes, such as targeting virions and viral components for elimination. These exciting findings have encouraged studies on the ability of autophagy to restrict HIV. However, the role of autophagy in HIV infection remains unclear. Whereas some reports indicate that autophagy is detrimental for HIV, others have claimed that HIV deliberately activates this pathway to increase its infectivity. Moreover, these contrasting findings seem to depend on the cell type investigated. Here, we show that autophagy poses a hurdle for HIV replication, significantly reducing virion production. However, HIV-1 uses its accessory protein Nef to counteract this restriction. Previous studies have indicated that Nef affects autophagy maturation by preventing the fusion between autophagosomes and lysosomes. Here, we uncover that Nef additionally blocks autophagy initiation by enhancing the association between BECN1 and its inhibitor BCL2, and this activity depends on the cellular E3 ligase PRKN. Remarkably, the ability of Nef to counteract the autophagy block is more frequently observed in pandemic HIV-1 and its simian precursor SIV$_{cpz}$ infecting chimpanzees than in HIV-2 and its precursor SIV$_{smm}$ infecting sooty mangabeys. In summary, our findings demonstrate that HIV-1 is susceptible to autophagy restriction and define Nef as the primary autophagy antagonist of this antiviral process.

Abbreviations: 3-MA: 3-methyladenine; ACTB: actin, beta; ATG16L1: autophagy related 16 like 1; BCL2: bcl2 apoptosis regulator; BECN1: beclin 1; cDNA: complementary DNA; EGFP: enhanced green fluorescence protein; ER: endoplasmic reticulum; Gag/p55: group-specific antigen; GFP: green fluorescence protein; GST: glutathione S transferase; HA: hemagglutinin; HIV: human immunodeficiency virus; IP: immunoprecipitation; MAP1LC3B/LC3B: microtubule associated protein 1 light chain 3 beta; Nef: negative factor; PRKN: parkin RBR E3 ubiquitin ligase; PtdIns3K: phosphatidylinositol 3 kinase; PtdIns3P: phosphatidylinositol 3 phosphate; PTM: post-translational modification; RT-qPCR: reverse transcription followed by quantitative PCR; RUBCN: rubicon autophagy regulator; SEM: standard error of the mean; SERINC3: serine incorporator 3; SERINC5: serine incorporator 5; SIV: simian immunodeficiency virus; SQSTM1/p62: sequestosome 1; TFEB: transcription factor EB; UVRAG: UV radiation resistance associated gene; VSV: vesicular stomatitis virus; ZFYVE1/DFCP1: zinc finger FYVE-type containing 1.

Introduction

Macroautophagy (hereafter autophagy) is a survival pathway activated in response to stress to target cargo such as malfunctioning proteins and organelles for lysosomal degradation [1,2]. This process is critical for cellular homeostasis since it allows the coordinated degradation and recycling of cellular components while providing an alternative source of energy and nutrients. In fact, defects in eliciting proper autophagic responses have been associated with many cancers, neuropathologies, and cardiovascular disorders [3–9].

Autophagy comprises more than 30 autophagy-related (ATG) genes that are highly conserved in all eukaryotes. These molecules work in the concerted formation of double-membrane vesicles (autophagosomes) that ultimately fuse with lysosomes for the degradation of their cargo. Autophagy consists of three basic stages: initiation, elongation, and maturation (Figure S1). In the initiation phase, BECN1/Beclin1 dissociates from its inhibitor BCL2 to facilitate the formation of phagophores through the activation of class III PtdIns3K complex I [10–13]. This phase involves the isolation of cellular membranes – mainly from the ER [13,14] – where cargo is targeted

---

(Figure S1). In the elongation step, the phagophore encloses the cargo in an autophagosome, which is coated by a processed version of MAP1LC3B/LC3B (hereafter LC3). Under normal conditions, LC3 is present as LC3-I: the autophagy-sensitive variant normally found dispersed in the cytosol. However, upon autophagy activation, LC3-I is lipidated by an E3-like enzymatic complex (E1: ATG7, E2: ATG3, and E3: ATG12–ATG5-ATG16L1) that adds phosphatidylethanolamine (PE) to its C-terminus, converting LC3-I into LC3-II: the autophagy-competent variant (Figure S1). This lipidation process takes place almost simultaneously with the formation of the phagophore and is dependent upon the activation status of BECN1 [15–17]. LC3-II is crucial for proper elongation and maturation of autophagosomes. Moreover, LC3-II recruits autophagy receptors such as SQSTM1/p62 that target cargo to these vesicles for their subsequent degradation [18–20]. Finally, in the maturation step, the autophagosome fuses with a lysosome, leading to the degradation of its contents, including SQSTM1 and LC3-II molecules found on the internal membrane of the vesicle [1,19,21–27] (Figure S1). Therefore, due to the fluctuations that these proteins suffer in response to autophagy, a common method to assess autophagy activation, progression and execution involves measuring the relative abundance of LC3-I, LC3-II and SQSTM1 [18,28,29].

Besides its role in cellular homeostasis, autophagy has recently become prominent as an antiviral defense mechanism [2,27]. Specifically, autophagy mediates the lysosomal degradation of viruses, impeding the progression of infections. In addition to this primary role, the autophagy-mediated breakdown of virus structures facilitates (a) their engagement with endosomal pattern recognition receptors for the activation of innate responses, and (b) their presentation through major histocompatibility complexes, thereby assisting in shaping the adaptive immune response against these pathogens [2,27,30,31]. These exciting findings have encouraged the pharmacological manipulation of autophagy as a therapeutic tool to combat viral infections [27,32]. However, many viruses have evolved strategies to subvert the degradative effects of autophagy by influencing the course of events that deliver viral molecules to autophagosomes [2]. This phenomenon is well-known for some herpesviruses, influenza viruses, poxviruses, and rotaviruses [2,27,33–35]. However, the interplay between autophagy and retroviruses [27,36,37], particularly HIV, is uncertain. Whereas some studies state that HIV deliberately activates autophagy to aid in the uncoating of its capsid to enhance infectivity [38,39], others have reported that capsid recognition by TRIM5/TRIM5α (tripartite motif-containing 5), a restriction factor that accelerates HIV uncoating and interferes in turn with reverse transcription [40–45], triggers autophagy to target incoming capsids for elimination [46]. In line with this restrictive effect of autophagy, other studies have reported that HIV inhibits the fusion between autophagosomes and lysosomes to prevent autophagy-mediated virion degradation [47–50]. These conflicting findings are exacerbated even further when studying the different cell types that HIV infects [51,52]. For instance, in dendritic cells, HIV-1 Env has been reported to downregulate autophagy [53,54], while autophagy is insensitive to HIV-1 Env in macrophages and CD4$^+$ T cells [51,52]. By contrast, secreted HIV-1 Env accelerates autophagy in uninfected bystander CD4$^+$ T cells [52,54,55]. Therefore, there is a critical need to elucidate the role of autophagy in the context of HIV infection to assess whether autophagy manipulation represents a feasible strategy to implement along with antiretroviral therapies.

Here, we show that autophagy causes a reduction in the expression levels of the HIV Gag/p55 structural protein in all the cell types investigated, leading to a defect in virion production. However, HIV counteracts this restriction with the viral protein Nef. Previous studies have defined Nef as an autophagy antagonist [38,49,50]. Specifically, Nef has been reported to act in an analogous manner as RUBCN, a potent autophagy inhibitor, hindering the ability of BECN1 associated with the class III PtdIns3K complex II to dock into autophagosomal membranes – which consequently prevents autophagy maturation [50]. Besides its ability to impair this late step, our studies demonstrate that Nef additionally blocks autophagy at the early, initiation stages. In particular, Nef prevents the lipidation of LC3 by enhancing the interaction between BECN1 and its inhibitor BCL2, and this activity requires the cellular E3 ligase PRKN. Nef is notorious for counteracting the innate effectors SERINC3 and SERINC5 as well as promoting immune evasion through the downregulation of the immune receptors CD4, CD28 and major histocompatibility complexes [56–65], facilitating, in turn, the spread of HIV. Therefore, Nef's ability to block autophagy represents an additional mechanism of immune evasion.

Results

Cell-specific differences in the sensitivity to autophagy stimuli

Previous studies have reported contrasting observations on the role of autophagy in HIV infection [32,38,39,47–49,51,52,54,55,66–68]. Many of these opposing findings are particularly evident when examining different HIV target cells, chiefly macrophages and CD4$^+$ T cells. For instance, autophagy activation in macrophages has been associated with increased virion production, while activation of this pathway has deleterious effects for HIV in other cell types [32,38]. Therefore, to understand the influence of autophagy on this virus, we first analyzed the response to autophagy stimuli of cells commonly used in HIV research, such as cell lines for CD4$^+$ T cells, monocytes, macrophages, primary CD4$^+$ T cells as well as the commonly used HEK293T cells. For this, we exposed these cells to nutrient starvation, mock transfections, or rapamycin to activate autophagy [18,69,70], and monitored the conversion of LC3-I into LC3-II, as well as the decay in SQSTM1, by western blotting at different time intervals. For simplicity, here we are showing results for rapamycin stimulation, but we observed similar findings in the presence of the other stimuli. Although autophagy is highly conserved, we found cell-type-specific differences in the kinetics and threshold to respond to autophagy triggers (Figure S2). For instance, in HEK293T cells, the activation of autophagy by

rapamycin was evident 4 h post-stimulation and as little as 1.3 µM of the drug was sufficient to detect an increase in LC3-II with a concomitant decrease in SQSTM1 (Figure S2A). By contrast, highly phagocytic cells, such as those of the myeloid lineage (i.e., THP-1 and THP-1-derived macrophages), showed inherently elevated basal levels of LC3-II [71]. Thus, to detect the transition of LC3-I to LC3-II, we needed higher doses of rapamycin and longer exposure to the drug (6 and 12 h) (Figure S2B). The response of Jurkat CD4+ T cells was intermediate between monocytes and HEK293T cells. In this case, the transition of LC3-I to LC3-II became evident after 6 h of rapamycin stimulation but required lower doses than the phagocytes. Similar to Jurkat cells, the activation of autophagy in primary CD4+ T cells became apparent 6 h after treatment with 4 µM of rapamycin. However, unlike Jurkat cells, primary CD4+ T cells exhibited high basal levels of LC3-II (Figure S2B). This phenotype was attributable to their activation and expansion with IL2 and anti-CD3 and anti-CD28 antibodies – which simulate conditions that would support HIV infection – before their exposure to autophagy stimuli. In fact, autophagy induction is generally observed upon CD4+ T cell activation, since it helps regulate energy metabolism during their differentiation to an effector phenotype [72–76]. In conclusion, these observations indicate that the basal levels of autophagy, as well as the stress threshold to trigger this pathway, differ in a cell-type-specific manner. Accordingly, we minimized the presence of external stressors – particularly for highly susceptible cells (i.e., HEK293T) – by replacing the cell medium regularly to better monitor the autophagic response to HIV in these distinct cellular environments.

Autophagy is activated in response to HIV, but the virus uses Nef to hinder autophagy progression

Since HEK293T cells are commonly used in HIV research, exhibit high transfection efficiency, and respond very quickly to autophagy stimuli, we initially used these cells to assess the interplay between autophagy and HIV-1 NL4-3, as well as mutants of this molecular clone. As controls, we included an empty retroviral vector, mock-treated cells, and cells treated with rapamycin (4 µM) for 4 h. We harvested the cells 48 h post-transfection and analyzed the lysates by western blot for the expression of HIV Gag (p55 and p24), ACTB/β-actin, and the autophagy markers LC3 and SQSTM1. As expected, the presence of cytosolic DNA triggered autophagy [77–79], and this was predominantly evident in the empty retroviral vector control, where we detected a significant conversion of LC3-I into LC3-II and a decrease in SQSTM1 (Figure 1A). By contrast, mock-treated cells showed higher levels of SQSTM1 and LC3-I over LC3-II, reflecting minimal activation of autophagy. Consistent with our previous observations, cells stimulated with rapamycin displayed a remarkable increase in LC3-II and a parallel reduction in SQSTM1 (Figure 1A). Contrary to the empty retroviral vector control, NL4-3-transfected cells showed a defect in the transition of LC3-I into LC3-II, and, in consequence, higher levels of SQSTM1. However, this impairment in autophagy progression was lost in the absence of a functional *nef* gene, since cells transfected with the NL4-3 Δ*nef* proviral DNA had a similar autophagy activation pattern as the cells transfected with the empty retroviral vector: rapid emergence of LC3-II and a significant decrease in SQSTM1. Moreover, we observed a defect in Gag expression in these cells (Figure 1A; red arrows). We consistently obtained similar findings in all four biological replicates, in which we measured the progression of autophagy by calculating the LC3-II:I ratio relative to the empty retroviral vector (Figure 1A; graph). Samples where the relative LC3-II:I ratios were <1 represent conditions in which autophagy had not been activated (i.e., mock) or where autophagy had been impaired. By contrast, samples where the relative LC3-II:I ratios were equal or >1 represent conditions of autophagy activation. Consistent with previous reports [38,49,50], our findings show that HIV-1 NL4-3 clones harboring a functional *nef* gene reduce autophagy progression. However, unlike earlier studies, our results indicate that Nef additionally affects the initiation stages of this pathway, reducing LC3-I-to-LC3-II conversion.

To investigate the reproducibility of this phenotype in HIV target cells, we infected Jurkat CD4+ T cells, THP-1-derived macrophages, and primary CD4+ T cells with wild type HIV-1 NL4-3 or NL4-3 Δ*nef*. In the case of the macrophage infection, we VSV-G pseudotyped NL4-3 Δ*env* and NL4-3 Δ*env*Δ*nef* to allow the infection of these cells. We collected cell lysates at different time intervals to assess Gag, Nef, LC3, SQSTM1, and ACTB levels, and we calculated the ratios of LC3-II:I relative to the first time point. This normalization allowed us to compare the effect of HIV on autophagy among the different cell types. Although macrophages and T cells differ in their sensitivity to autophagy triggers, and they exhibit differences in their basal levels of LC3-II (Figure S2B), the impact of Nef on autophagy activation/progression remained evident in these cells. In the case of the Jurkat cells, the accumulation of LC3-I, and thus the defect in the emergence of LC3-II, was obvious at 48 h post-infection, which coincided with the time when Nef expression became apparent. However, cells infected with *nef*-deficient viruses showed normal transition of LC3-I to LC3-II, faster decline of SQSTM1 over time, and lower Gag expression levels compared to cells infected with the wild type virus (Figure 1B; western blots). We obtained similar results in all 3 biological replicates, in which we found a significant reduction in the relative LC3-II:I ratios for cells infected with *nef*-competent viruses, particularly at the later time points (Figure 1B; graph).

We had similar observations in macrophages. Although these cells have inherently high basal levels of LC3-II, and the VSV-G pseudotyped viruses are restricted to one cycle of infection, macrophages infected with viruses harboring a functional *nef* gene showed detectable levels of LC3-I compared to cells infected with *nef*-defective viruses (Figure 1C; red arrows). This result caused, in turn, a reduction in the LC3-II:I ratios. The Nef-mediated impairment in the emergence of LC3-II was also accompanied by higher levels of SQSTM1, indicating that the presence of Nef hindered autophagy. Accordingly, the levels of Gag (p55) normalized to ACTB were lower in cells infected with NL4-3 Δ*env*Δ*nef* than NL4-3 Δ*env*–infected cells (Figure 1C). Consistent with the data obtained in HEK293T
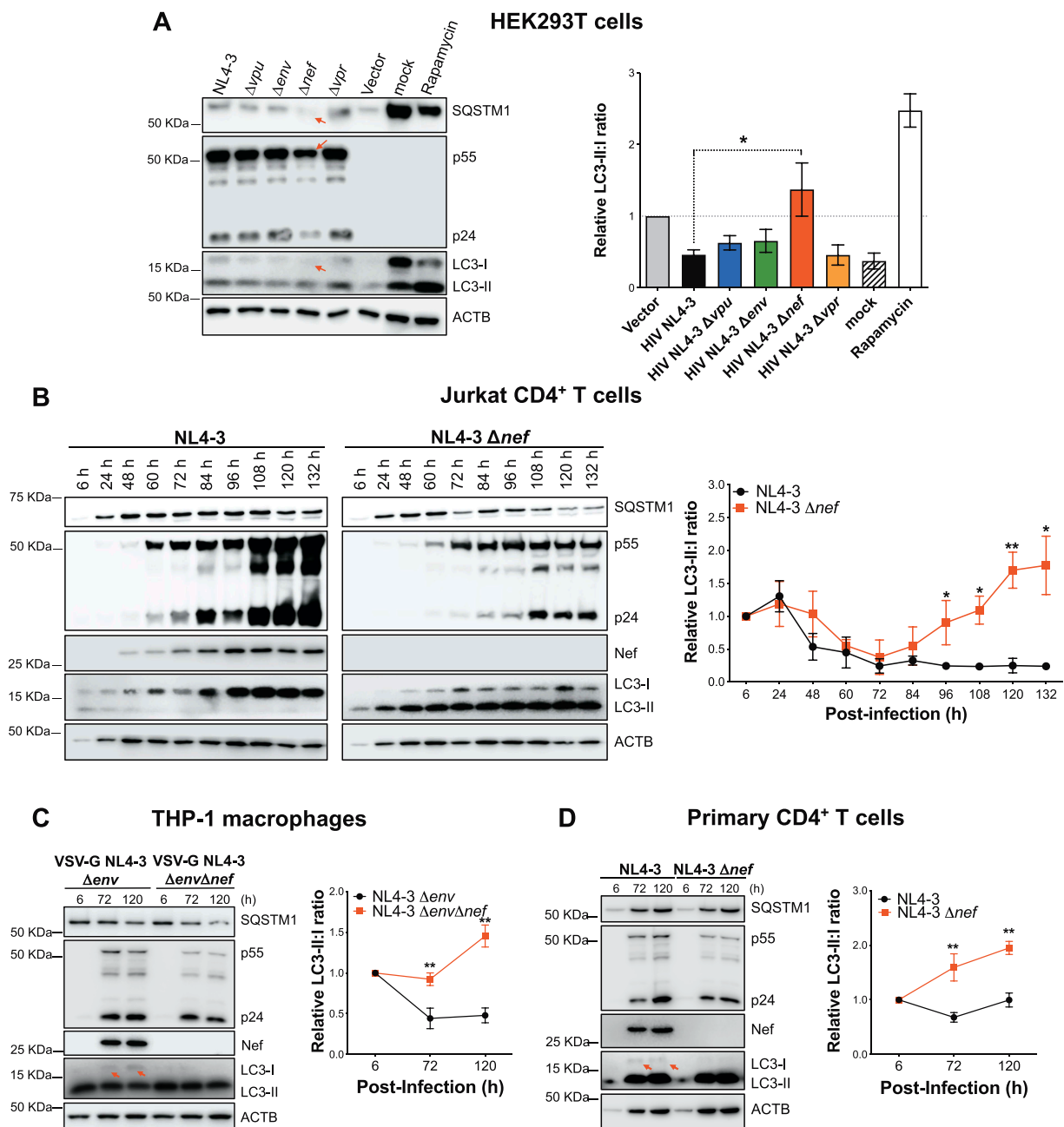
Figure 1. HIV uses Nef to block autophagy. (A) Left panel: HEK293T cells were transfected with the full-length proviral DNA of HIV-1 NL4-3, different mutants of this molecular clone (Δvpu, Δenv, Δnef and Δvpr), or an empty retroviral vector. As controls for autophagy, cells were treated with 4 μM of rapamycin or mock (DMSO) for 4 h. 48 h post-transfection, cells were lysed and analyzed by western blot for SQSTM1, Gag (p55 and p24), LC3 and ACTB/β-actin. Right Panel: Densitometric analyses were performed to determine the ratio of LC3-II over LC3-I relative to the empty vector control. Data represent the mean and standard error of the mean (SEM) from 4 independent biological replicates. (B) Jurkat CD4^{+} T cells, (C) THP-1-derived macrophages and (D) primary CD4^{+} T cells were infected with 100 ng of p24 equivalents of HIV-1 NL4-3 or HIV-1 NL4-3 Δnef. In the case of macrophages, infections were performed with VSV-G pseudotyped HIV-1 NL4-3 Δenv or HIV-1 NL4-3 ΔenvΔnef. Cell lysates were collected at the indicated time intervals and analyzed by western blot for SQSTM1, Gag (p55 and p24), Nef, LC3, and ACTB (left panels). The right panels correspond to the mean and SEM of 3 independent experiments showing the ratios of LC3-II:I over time relative to the first data point, which were calculated by densitometric analyses. *: $p \leq 0.05$; **: $p \leq 0.01$. Red arrow in panel A indicates decreased Gag and SQSTM1 levels as well as rapid LC3-I-to-LC3-II transition. Red arrows in panels C and D indicate the accumulation of LC3-I.

and Jurkat cells, the differences in the relative LC3-II:I ratios were statistically significant between *nef*-competent and *nef*-defective viruses (Figure 1C; graph).

As indicated earlier, primary CD4^{+} T cells exhibit high autophagy activation, reflected by elevated LC3-II (Fig. S2B). Although the prominent expression of LC3-II complicated the detection of LC3-I, the Nef-mediated impairment in

autophagy flux was still noticeable in these cells, since we detected LC3-I in NL4-3-infected cells, but not in cells infected with NL4-3 Δnef (Figure 1D; red arrows). In conclusion, by measuring autophagy status through the calculation of the relative ratios of LC3-II:I, we have been able to compare the effects of HIV on this pathway across different cell types. Our data indicate that, although their basal autophagy

activation and the threshold to trigger this cascade differ, cells – including primary CD4^{+} T cells – respond to HIV infection/transfection by inducing autophagy. However, HIV uses the accessory protein Nef to intersect with this pathway.

Autophagy causes a defect in particle production that is counteracted by Nef

Our results showed an association between Nef-mediated inhibition of autophagy and Gag expression levels. Because Gag is the major driver of virion assembly and release, we consequently assessed whether autophagy causes detrimental effects on Gag and infectious virus production. Since we observed the effects of HIV on autophagy in all cell types, we chose HEK293T cells, which are highly sensitive to auto-phagy stimuli – yet the pathway remains responsive to HIV – for these studies. We transfected HEK293T cells with wild-type and *nef*-defective HIV-1 NL4-3 proviral constructs. We replaced the cell medium 24 h later and treated the cells with increasing concentrations of rapamycin (0–4 μM) for 12 h to trigger autophagy. Subsequently, we assessed the effect of autophagy activation on virion production by measuring the amount of capsid p24 present in the culture supernatant by p24 antigen-capture ELISA. We expressed particle release relative to the no-rapamycin treatment as the percentage of maximal virus production for each virus (wild-type and Δ*nef*), as we previously reported [80–83]. By comparing the effect of rapamycin-induced autophagy within viruses – instead of between viruses – we excluded (a) any differences in transfection efficiencies between these proviral constructs, and (b) any other processes that Nef may be influencing, such as infectivity enhancement through SERINC3 and SERINC5 antagonism [56]. We found that rapamycin-induced auto-phagy caused a dose-dependent defect in virion release for the *nef*-deleted NL4-3 virus (Figure 2A; top panel), which was also associated with a dose-dependent decrease in Gag (Figure 2A; bottom panel). By contrast, wild type NL4-3 only exhibited a partial decrease in particle release at the higher concentrations of rapamycin and minimal defects in Gag (Figure 2A). Of note, whereas in cells transfected with NL4-3 Δ*nef* autophagy proceeded uninterruptedly (since there was a transition of LC3-I to LC3-II in response to rapamycin), autophagy flux was halted in cells transfected with wild type NL4-3, since there was an impairment in the emergence of LC3-II (Figure 2A; bottom panel). Remarkably, this defect in virion production and Gag expression became restored when we provided *nef in trans* (Figure 2B), under-scoring that the Nef-mediated block of autophagy protects from any detrimental effect autophagy exerts on HIV replica-tion. To corroborate that the reduction in particle production caused by rapamycin in NL4-3 Δ*nef* is due to autophagy activation and not to other effects caused by this drug, we performed competition experiments between rapamycin and 3-methyladenine (3-MA), a compound that specifically blocks autophagy by preventing BECN1-associated class III PtdIns3K complex I activation [84,85]. As expected, we observed a dose-dependent decrease in virion production for *nef*-defective NL4-3 with increasing concentrations of rapamycin. However, the addition of 3-MA (3 mM) restored

Gag and particle release for this virus, and this finding was associated with an accumulation of LC3-I (Figure 2C; bottom panel). We obtained similar results after knocking down *BECN1* by silencing RNA (siRNA) (Figure 2D). Consistent with its role in phagophore formation [10–12], depletion of BECN1 arrested autophagy activation, reflected by retention in LC3-I, since this factor is critical for the biogenesis of LC3-II (Figure 2D; right panel). Accordingly, the overall Gag levels for NL4-3 Δ*nef* were higher than in the si-control cells, affording, in turn, significantly higher virion production (Figure 2D). We also observed this phenomenon in Jurkat CD4^{+} T cells. In this case, we infected cells with wild-type and *nef*-defective HIV-1 NL4-3, and, 24 h later, we replaced and supplemented the medium with rapamycin in an analogous manner as for the assays in HEK293T cells. Consistent with our previous observations showing that Jurkat cells are more resistant to autophagy activation than HEK293T cells (Figure S2B), we found less autophagy activation in these cells, and thus, less restriction of HIV. However, in line with our pre-vious findings (Figure 2A-D), the *nef*-deficient virus remained more vulnerable to autophagy-mediated clearance than wild type NL4-3 (Figure 2E). Therefore, these results further corroborate that autophagy poses a hurdle for HIV by affecting Gag levels, but the virus uses Nef to overcome this barrier. To rule out that the autophagy-dependent defect in Gag is not an artifact due to transfection or infection variabilities, we assessed *gag* mRNA levels in HEK293T cells at 6 and 18 h post-transfection, and we normalized the levels of *gag* mRNAs to those of HIV-1 NL4-3 at the first data point. We observed no significant fluctuations in *gag* mRNAs (Figure S3A), reflecting similar transfection efficiencies for wild type and NL4-3 Δ*nef*. Hence, these findings indicate that autophagy impacts Gag, particularly in the absence of a functional *nef* gene. Since we observed the autophagy-mediated defect in Gag and particle production in HEK293T cells, in which we provided NL4-3 clones through transfections bypassing any entry and integration steps, we can conclude that the autophagy block takes place at a post-integration event in the HIV replication cycle.

Nef impairs the lipidation of LC3 and, subsequently, autophagosome formation

To understand how Nef blocks autophagy, we first confirmed that the relative increase in LC3-I is also observed in Nef-only expressing cells, in the absence of the rest of the NL4-3 genome. For this, we monitored autophagy in HEK293T cells transfected with pCGCG-EGFP, an expression vector that codes for EGFP from an internal ribosomal entry site (IRES), and pCGCG-NL4-3-Nef-EGFP [80,81]. We replaced the cell medium 8 h post-transfection, and either (a) we treated 48 h later the cells with increasing concentrations of rapamycin for 4 h, or (b) we starved them for 4 d. We harvested cells after these treatments and analyzed autophagy by assessing the levels of SQSTM1 as well as LC3-II:I by western blot. Consistent with our observations with the full-length NL4-3 provirus, Nef, but not the empty pCGCG vector control, arrested autophagy progression reflected by low LC3-II:I ratios and more steady SQSTM1 levels, and we observed this obstruction in all three biological replicates under
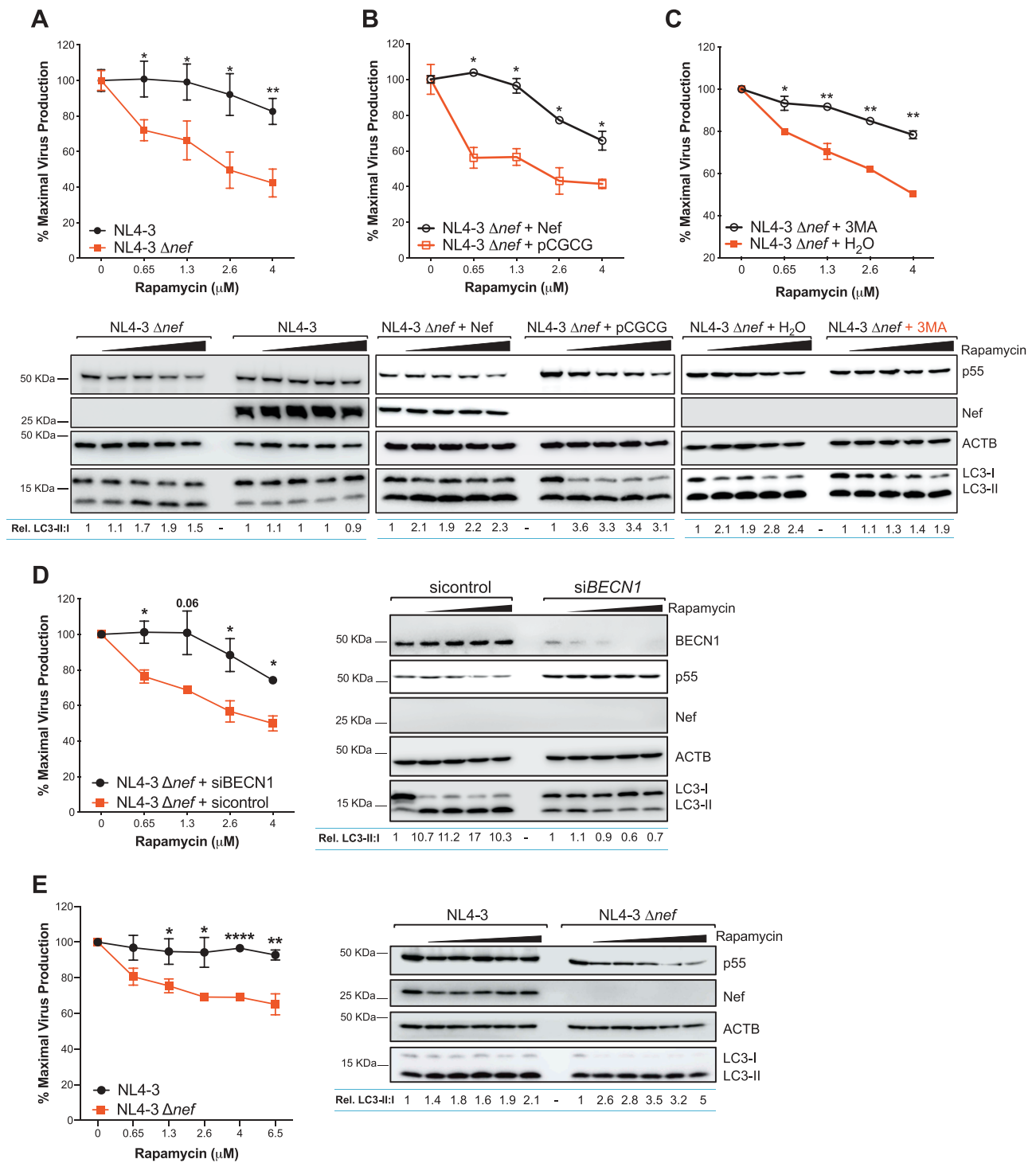
Figure 2. Autophagy limits virion production in *nef*-defective HIV. (A) Top panel: HEK293T cells were transfected with the full-length proviral DNA of HIV-1 NL4-3 or NL4-3 Δ*nef* and treated with the indicated concentrations of rapamycin for 12 h. The percentage of maximal virus production was then measured by the accumulation of HIV p24 in the culture supernatant relative to the no-rapamycin treatment for each virus. Bottom panel: Cells were also analyzed by western blot for Gag p55, Nef, ACTB, and LC3. (B) Top panel: HEK293T cells were transfected with the proviral DNA of HIV-1 NL4-3 Δ*nef* and trans-complemented with either NL4-3 *nef* or an empty vector. Similar to panel A, cells were treated with increasing concentrations of rapamycin for 12 h, and the percentage of maximal virus production relative to the no-rapamycin treatment was measured as explained above. Bottom panel: Cell lysates were analyzed as in panel A. (C) Top panel: HEK293T cells were transfected with the proviral DNA of HIV-1 NL4-3 Δ*nef* and stimulated with increasing concentrations of rapamycin for 12 h. Next, cells were either treated with 3-MA (3 mM) or water 4 h before measuring the percentage of particle release. Bottom panel: Cells were also analyzed by western blot as in panel A. (D) Left panel: HEK293T cells were transfected with either siRNA for *BECN1* or a control siRNA. 24 h later, the cells were transfected again with the proviral DNA of HIV-1 NL4-3 Δ*nef* and treated with rapamycin for 12 h. Next, the percentage of maximal virus production was measured as indicated above. Right panel: Cell lysates were also analyzed for BECN1, Gag p55, Nef, ACTB, and LC3. (E) Left panel: Jurkat CD4^{+} T cells were infected with 100 ng of p24 equivalents of HIV-1 NL4-3 or HIV-1 NL4-3 Δ*nef*. 24 h later, the cell medium was replaced and supplemented with different concentrations of rapamycin. 12 h later, the percentage of maximal virus production was measured as detailed above. Right panel: cell lysates were analyzed as in panel A. In each case, the percentage of maximal virus production is indicated as the mean and SEM from 4 independent biological replicates. *: $p \leq 0.05$; **$p \leq 0.01$; ****$p \leq 0.0001$. Numbers underneath the blots indicate the ratio of LC3-II:I relative to the no-rapamycin treatment.

rapamycin and starvation-induced autophagy (Figure 3A,B; bar graphs). The common denominator of rapamycin and starvation is the inactivation of the mechanistic target of rapamycin complex 1 (MTORC1) [86–88]. Therefore, our findings indicate that Nef antagonizes autophagy at a step between MTORC1 and the lipidation of LC3.

Although our data show that Nef causes the accumulation of LC3-I, this result may be due to an indirect effect of Nef on the expression of *LC3B*. To rule this out, we monitored the mRNA levels of *LC3B* in the presence and absence of Nef by RT-qPCR. We also assessed the expression levels of *ATG16L1*, one of the enzymes that form the E3-like complex involved in the lipidation of LC3, which is mainly regulated by TFEB (transcription factor EB). TFEB is a master regulator of autophagy genes that, besides other transcription factors, also modulates *LC3B* expression [89–91], and has recently been reported to be inhibited by Nef [49]. Therefore, we evaluated whether Nef affects the expression of *LC3B* and if this effect is dependent on TFEB. We transfected HEK293T cells with pCGCG-EGFP and NL4-3 *nef*. We examined *LC3B* and *ATG16L1* mRNA levels at 6, 24, and 48 h post-transfection, and we indicated their expression relative to the 6 h data point as mRNA fold change after normalization to *GAPDH* and *GFP* (to correct for transfection efficiencies). As mentioned earlier, cytosolic DNA triggered autophagy, since we detected a peak in *LC3B* and *ATG16L1* mRNAs 6 h post-transfection in both the empty vector and NL4-3 *nef*-transfected cells. Accordingly, this effect slowly disappeared upon replacing the cell medium, indicated by a steady decline in the mRNA levels of *ATG16L1* and *LC3B* (Figure 3C; lines with open symbols). However, while we detected no differences in the expression of *ATG16L1* (Figure 3C; blue lines), we found a ~ 2-fold reduction in *LC3B* mRNA in Nef-expressing cells, although it did not reach statistical significance (Figure 3C, green lines). In line with these results, we found a similar downregulating effect in *LC3B* in the context of the full-length NL4-3 provirus (Figure S3B). Hence, these observations rule out a role for Nef in the upregulation of *LC3B*. On the contrary, it seems that Nef downregulates *LC3B* as an additional mechanism to block autophagy, but likely in a TFEB-independent manner.

To confirm that a defect in LC3 lipidation causes the Nef-mediated increase in LC3-I, we assessed LC3-I-to-LC3-II transition in HEK293T cells transfected with wild type NL4-3 and Δ*nef* in the presence of chloroquine, a lysosomal inhibitor that also halts autophagy maturation. As expected, the addition of chloroquine (60 μM) caused a significant increase in LC3-II in all samples, since autolysosomal function is impaired and in this scenario LC3-II is more stable [18]. Accordingly, the SQSTM1 levels remained steady. However, we still observed the increase in LC3-I in samples where either autophagy remained inactive (mock) or where it had been intersected (Nef) (Figure 3D; red arrows). Remarkably, Gag levels became restored under these conditions, even for the *nef*-deficient virus, suggesting that autophagy targets Gag, consequently impacting virion assembly and production (Figure 3D; right blot).

We corroborated that Nef obstructs LC3 lipidation and, as a consequence, autophagosome formation by flow cytometry assays. For this, we employed the pC3-EGFP-LC3B expression construct. Upon autophagy activation, the fusion protein EGFP-LC3B is associated to phagophores and autophagosomes rather than distributed in the cytosol. This membrane association makes autophagosome bound EGFP-LC3B resistant to saponin elimination. In consequence, upon saponin treatment, cytosolic EGFP-LC3-I is washed out, so any EGFP signal detected corresponds to phagophore- and autophagosome-bound EGFP-LC3-II. To avoid any interference in the EGFP signal between pCGCG and EGFP-LC3B, we used pcDNA5 instead of pCGCG-EGFP as the empty vector control and pCI-NL4-3-Nef-HA instead of pCGCG-NL4-3-Nef-EGFP in our transfections. As expected, the inhibitory effect that 3-MA exerts on autophagy led to considerably lower EGFP signal than in rapamycin-treated cells. Consistent with the data in Figure 3A,B,D, showing that Nef halts the lipidation of LC3, Nef reduced autophagosome formation, with significantly lower levels of membrane-associated EGFP-LC3B than the rapamycin or vector controls (Figure 3E). We further confirmed these findings by fluorescence microscopy. We used the EGFP-LC3B construct again to visualize autophagosome structures through EGFP-LC3B puncta, a phenomenon generated when LC3-I is converted into LC3-II [18]. For this, we co-transfected HEK293T cells with EGFP-*LC3B* and either an empty vector (pcDNA5), an irrelevant gene (HA-*GST*), or NL4-3 *nef*-HA. 48 h post-transfection, we treated cells with rapamycin (4 μM) for 4 h, and subsequently imaged them for HA (DyLight-550; red), EGFP-LC3B (green) and the nuclei (DAPI; blue). As a negative control, we treated rapamycin-stimulated cells with 3-MA (3 mM). Consistent with its role in autophagy activation, rapamycin potently triggered the formation of autophagosomes reflected by multiple EGFP-LC3B puncta (Figure 3F; top panel). By contrast, treatment with 3-MA prevented the lipidation of LC3, and in consequence, we observed LC3-I distributed throughout the cytosol (Figure 3F; middle panel). As expected, HA-GST had no impact on the progression of autophagy, since we readily detected LC3 puncta (Figure 3F; bottom panel). Consistent with the data in Figure 3E, expression of Nef caused a similar phenotype as 3-MA since we mainly found EGFP-LC3B dispersed in the cytosol with only a few puncta (Figure 3G; cells with white borders). Quantification of puncta in 20 randomly selected cells confirmed a significant reduction of autophagosomes by Nef (Figure 3H). Accordingly, ZFYVE1/ DFCP1 puncta – a marker for autophagosome initiation – was also significantly diminished in Nef-expressing cells, even under conditions of rapamycin-induced autophagy (Figure S4A-S4C). ZFYVE1 shuttles from Golgi to the ER upon autophagy activation and facilitates the creation of a membrane hub for the accumulation of autophagy proteins. Remarkably, its translocation to phagophore structures depends on class III PtdIns3K complex I function [92]. Hence, these results support that Nef interferes with autophagy initiation, impairing efficient conversion of LC3-I into LC3-II, and in turn, in autophagosome biogenesis.

Nef enhances the association between BECN1 and BCL2 to prevent the formation of autophagosomes

Our data consistently show that Nef impacts autophagy initiation, affecting the transition of LC3-I into LC3-II. To elucidate
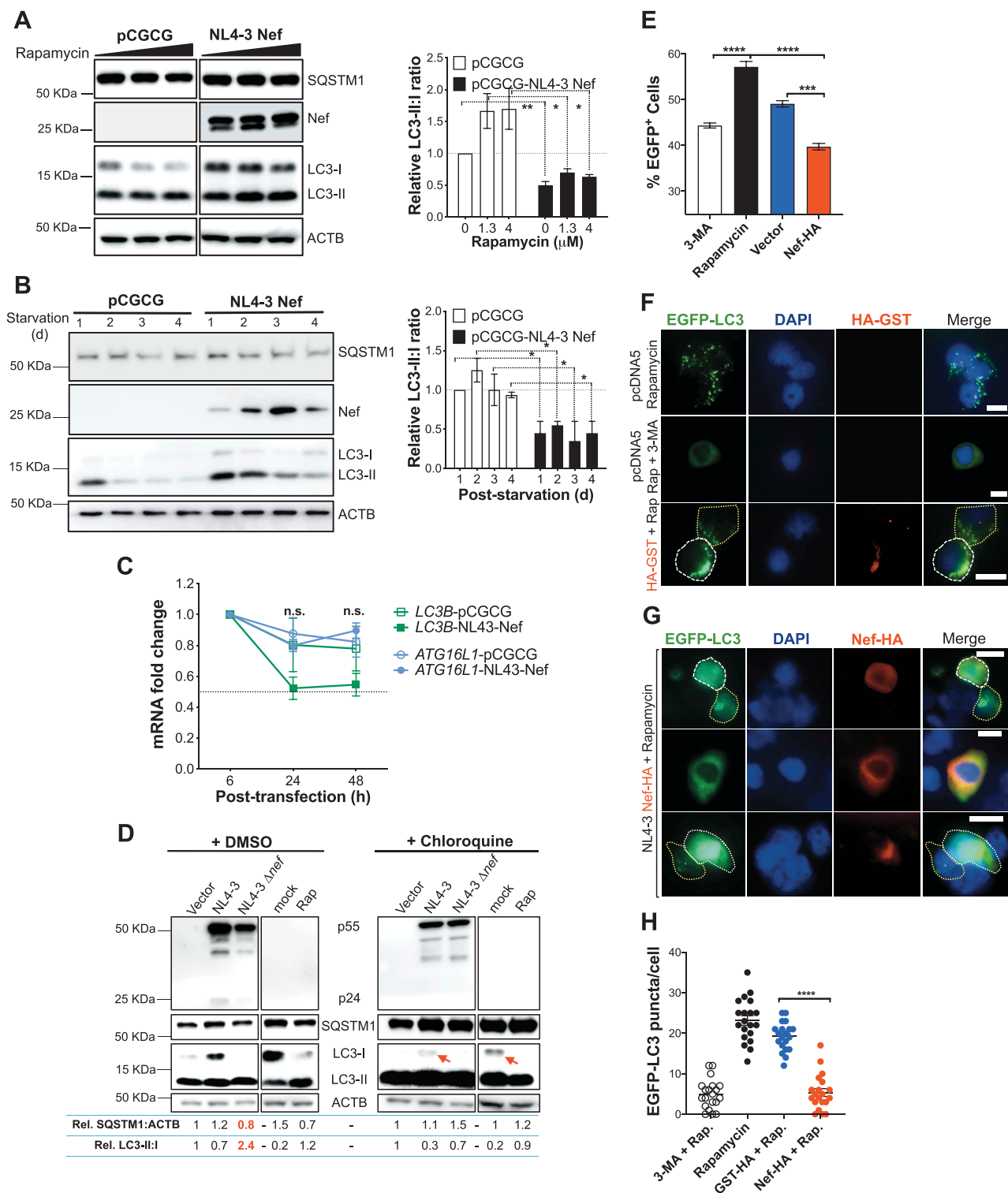
Figure 3. Nef impairs the lipidation of LC3, affecting autophagosome formation. (A, B) HEK293T cells were transfected with NL4-3 *nef* or an empty vector. 48 h later, cells were (A) exposed to the indicated concentrations of rapamycin, or (B) starved for the selected times. Left panels: Cells were analyzed by western blot for SQSTM1, Nef, LC3, and ACTB. Right panels: Data represent the mean and SEM of the ratios of LC3-II over LC3-I relative to the empty vector control (without rapamycin or at 1 d post-starvation, respectively) from 3 independent biological replicates. (C) HEK293T cells were transfected with NL4-3 *nef* or an empty vector. Next, the mRNA levels of *LC3B* and *ATG16L1* were assessed at the selected time points by RT-qPCR and expressed as fold change after normalization to *GAPDH* and *GFP*. Data represent the mean and SEM from 3 independent biological replicates. The dashed line represents cutoff for biologically relevant differences. (D) HEK293T cells were transfected with HIV-1 NL4-3 or NL4-3 Δ*nef* proviral constructs. Cells treated with rapamycin or transfected with an empty retroviral vector were included as controls. 24 h later, cells were treated with DMSO or chloroquine (60 μM) for 12 h. Next, cells were analyzed by western blot for Gag (p55 and p24), SQSTM1, LC3, and ACTB. The SQSTM1:ACTB and LC3-II:I ratios relative to the vector control are provided underneath the blots. (E) HEK293T cells were co-transfected with EGFP-*LC3B* and an empty vector or NL4-3 *nef*-HA. As controls, cells were also treated with rapamycin (4 μM) and 3-MA (3 mM). 48 h post-transfection, cells were analyzed by flow cytometry for autophagosome-associated EGFP-LC3B. Data correspond to the mean and SEM of the percentage of EGFP+ cells from 3 independent experiments. (F, G) HEK293T cells were co-transfected with EGFP-*LC3B* and either an empty vector, *GST*-HA (F) or NL4-3 *nef*-HA (G). Cells were exposed for 4 h to rapamycin (4 μM) in the presence and absence of 3-MA (3 mM) prior to microscopy visualization. Next, cells were stained for GFP (green), HA (DyLight-550; red) and the nuclei (DAPI; blue). (H) Data correspond to the mean and SEM of EGFP-LC3B puncta present in 20 randomly selected cells for each experimental condition. *: $p \leq 0.05$; **: $p \leq 0.01$; ***: $p \leq 0.001$; ****: $p \leq 0.0001$; n.s. not significant. Red arrows: accumulation of LC3-I. White scale bar: 10 μm. Cells surrounded by white borders are HA+.

the mechanism by which Nef achieves this, we explored the following hypotheses: (a) Nef interacts with LC3, physically preventing its lipidation; (b) Nef interferes with the enzymatic complex involved in the lipidation of LC3 (E1: ATG7, E2: ATG3 and E3: ATG12–ATG5-ATG16L1), either through direct interaction or by affecting their expression or subcellular localization; or (c) Nef blocks steps before LC3 lipidation in the autophagy cascade, such as activation of ULK1 (unc-51 like autophagy activating kinase 1) or BECN1. To investigate these possible scenarios, we assessed the ability of NL4-3 Nef to physically interact with any of these proteins in HEK293T cells by co-immunoprecipitation, and we monitored any changes in their expression pattern by western blot. We observed no evident interactions between Nef and any of these autophagy molecules (Figure S5A). Likewise, we detected no evident fluctuations in their steady-state levels either, even under rapamycin stimulation (Figure 4A). However, we observed a change in the migration pattern of BCL2 in cells expressing Nef, reflecting changes in BCL2's post-translational modifications (PTMs) (Figure 4A; red asterisks).

BCL2 is an inhibitor of autophagy by sequestering BECN1 [93–95]. In particular, BCL2 uses its BH3 domain to associate with the BH3 domain of BECN1, facilitating BECN1 homodimerization and, in consequence, preventing BECN1 from forming the class III PtdIns3K complex I, which is responsible for generating phosphatidylinositol 3-phosphate (PtdIns3P) [95–97]. PtdIns3P is an essential molecule for the formation of phagophore structures and the recruitment of the enzymatic complex required for the lipidation of LC3 [17] (Figure 4B). Therefore, the release of BECN1 from BECN1-BCL2 complexes is essential for the initiation of the autophagic response. This association is regulated by a myriad of PTMs, among them those that regulate BCL2 [13]. For instance, phosphorylation of BCL2 at Ser70 causes its dissociation from BECN1, allowing BECN1 to form the PtdIns3K complex I [98,99] (Figure 4B; top). Conversely, BCL2 mono-ubiquitination by the cellular E3 ligase PRKN enhances its interaction with BECN1 [100], inhibiting autophagy initiation and, in consequence, leading to a defect in the lipidation of LC3 (Figure 4B; bottom). To investigate how Nef affects BCL2 PTMs, we immunoprecipitated BCL2 from Nef-expressing HEK293T cells and cells transfected with the pCGCG-EGFP vector control and assessed BCL2 ubiquitination levels by probing membranes with a ubiquitin-specific antibody. As a negative control, we also probed membranes with anti-SUMO antibodies, since BCL2 has not been reported to harbor SUMO target sequences. We analyzed the phosphorylation status of BCL2 from the whole cell lysates using a p-Ser70-specific antibody. Consistent with our observations in Figure 4A, we found a different pattern in the migration of BCL2 between cells expressing Nef and the empty vector (Figure 4C; bottom blots). We also detected an intensification in p-BCL2 in the presence of Nef. However, we only noticed BCL2 mono-ubiquitination in Nef-expressing cells (Figure 4C, top blots). Although our ubiquitin-specific antibody did not discriminate between mono- and poly-ubiquitination, the relative size of the ubiquitin-containing band fitted with mono-ubiquitinated BCL2 (Figure 4C; red pound symbol). Since we found more ubiquitinated BCL2 in the presence of Nef, we next performed co-immunoprecipitation assays to investigate whether Nef promotes this PTM to increase the association between BECN1 and BCL2. Consistent with a role for Nef in intersecting autophagy at the initiation stages, we found >2-fold enhancement in the BECN1-BCL2 interaction in Nef-expressing HEK293T cells (Figure 4D). Remarkably, we consistently observed this phenomenon regardless of what molecule was pulled down, even when we overexpressed BECN1 (Figure 4D and S5B), and quantifications of the relative BECN1-BCL2 binding from 6 independent experiments supported these findings (Figure 4D; graph). To further corroborate that Nef blocks autophagy through BCL2, we assessed autophagy activation status, as well as its effect on virion production, under conditions of BCL2 inhibition. For this, we transfected HEK293T cells with the proviral HIV-1 NL4-3 and Δnef constructs. 24 h later, we replaced the cell medium, and treated the cells with increasing concentrations of rapamycin (0–4 μM) for 12 h, as described above, in the presence and absence of GX15-070 at its IC_{50} (3 μM). GX15-070 specifically inhibits the BCL2 BH3 domain, involved in the association with BECN1 [94,101], likely affecting BECN1-BCL2 interaction. As expected, the presence of Nef successfully impaired autophagy progression in cells treated with rapamycin. However, in the presence of GX15-070, we observed a significant increase in autophagy flux and a concomitant reduction in Gag and virion production, even in the absence of rapamycin stimulation (Figure 4E; right panel, compare lanes 1 and 6), reflecting Nef's inability to block the lipidation of LC3 (Figure 4E; see LC3 levels in the blots). Moreover, the fact that GX15-070 similarly restricted both wild type and nef-defective NL4-3, rather than causing additive effects for NL4-3 Δnef, supports that Nef uses BCL2 through its association with BECN1 to arrest autophagy progression (Figure 4E).

The Nef-mediated enhancement of BECN1-BCL2 interaction is PRKN-dependent

Since PRKN is the primary E3 ligase that mediates BCL2 mono-ubiquitination [100], we took advantage of the fact that HeLa cells are PRKN negative [102–104] and investigated whether this molecule is necessary for the Nef-dependent enhancement of BCL2's association with BECN1. For this, we performed additional co-immunoprecipitation assays for BCL2 and BECN1 in HEK293T cells, parental HeLa cells, and HeLa cells overexpressing PRKN-MYC, in the presence and absence of NL4-3 Nef. Consistent with our previous data, Nef enhanced the association between BECN1 and BCL2 by >2-fold in HEK293T cells. As expected, we observed no enhancement in this interaction in parental HeLa cells. However, providing PRKN-MYC in trans to HeLa cells expressing Nef restored the enrichment in the BECN1-BCL2 interaction (Figure 5A; top blots), and reduced the relative LC3-II:I ratios (Figure 5A; bottom blots), reflecting that PRKN is part of the mechanism by which Nef intersects with the autophagy machinery. We consistently observed these results in four independent experiments where we calculated the relative binding between BECN1 and BCL2 for each cellular scenario (Figure 5A; graph). To corroborate these findings, we performed loss-of-function studies by knocking down PRKN in HEK293T cells. Under these conditions, Nef no longer enhanced the association between
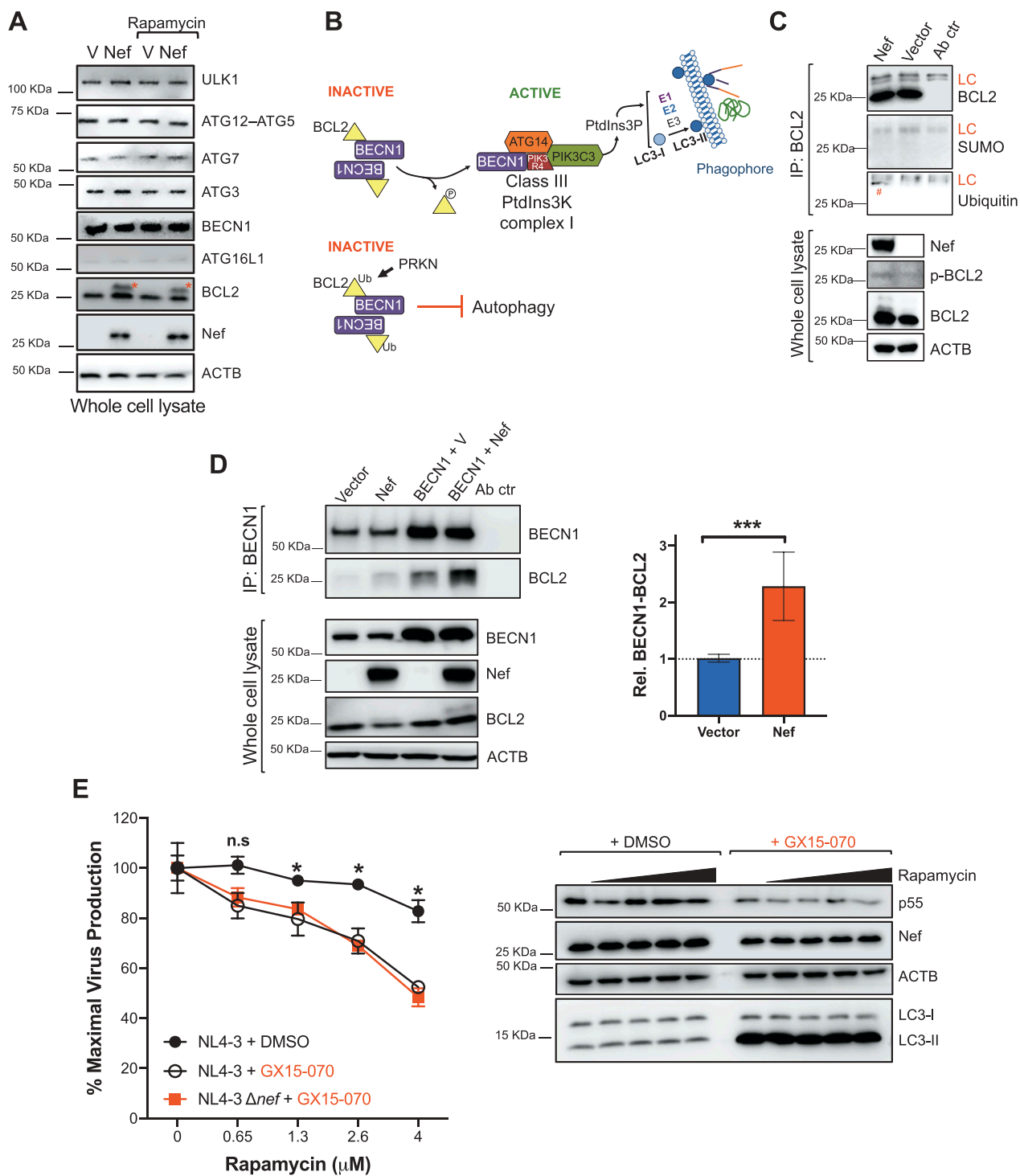
Figure 4. Nef enhances the association between BECN1 and BCL2 to arrest autophagy initiation. (A) HEK293T cells were transfected with NL4-3 *nef* or an empty vector. 48 h later, cells were exposed to rapamycin (4 μM) for 4 h. The cell lysates were analyzed by western blot to assess the expression levels of the proteins ULK1, ATG12–ATG5, ATG7, ATG3, BECN1, ATG16L1, BCL2, Nef, and ACTB. (B) Schematic diagram of the regulatory effect of BCL2 on the BECN1-dependent initiation of autophagy. (C) HEK293T cells were transfected with NL4-3 *nef* or an empty vector. 48 h later, BCL2 was immunoprecipitated from the cell lysates to assess its levels of ubiquitination and SUMOylation. The cell lysates were also analyzed by western blot to evaluate the levels of Nef, p-BCL2, BCL2, and ACTB. (D) HEK293T cells were co-transfected with *BECN1*-Flag and NL4-3 *nef* or an empty vector. 48 h later, the cell lysates were subjected to immunoprecipitation for BECN1. The pulldown fraction was then examined for the presence of BECN1 and BCL2. The cell lysates were also analyzed by western blot to assess the cellular levels of BECN1, Nef, BCL2, and ACTB. Graph: Data represent the mean and SEM of 6 independent biological replicates to calculate the relative binding between BECN1 and BCL2 obtained by densitometry analyses. (E) Left panel: HEK293T cells were transfected with the full-length proviral DNA of HIV-1 NL4-3 or NL4-3 Δ*nef*. 24 h later, the cell medium was replaced, and cells were treated for 12 h with either the indicated concentrations of rapamycin and DMSO or a combination of rapamycin and GX15-070 at its IC_{50} (3 μM), an inhibitor of BCL2. The percentage of maximal virus production relative to the no-rapamycin treatment was then measured for each virus and condition by the accumulation of HIV p24 in the culture supernatant. Data represent the mean and SEM of 3 independent biological replicates. Right panel: Cell lysates for samples transfected with the HIV-1 NL4-3 proviral construct were also analyzed for Gag p55, Nef, ACTB, and LC3. V: vector. Rel: relative. Ab ctr: cell lysates were incubated with the antibody used for the pulldown assays to exclude bands corresponding to the heavy and light chain (HC and LC) of the antibodies from the target proteins. Asterisk: differential migration pattern of BCL2. Pound sign: ubiquitinated BCL2. *: $p \leq 0.05$; *** $p \leq 0.001$; n.s. not significant.
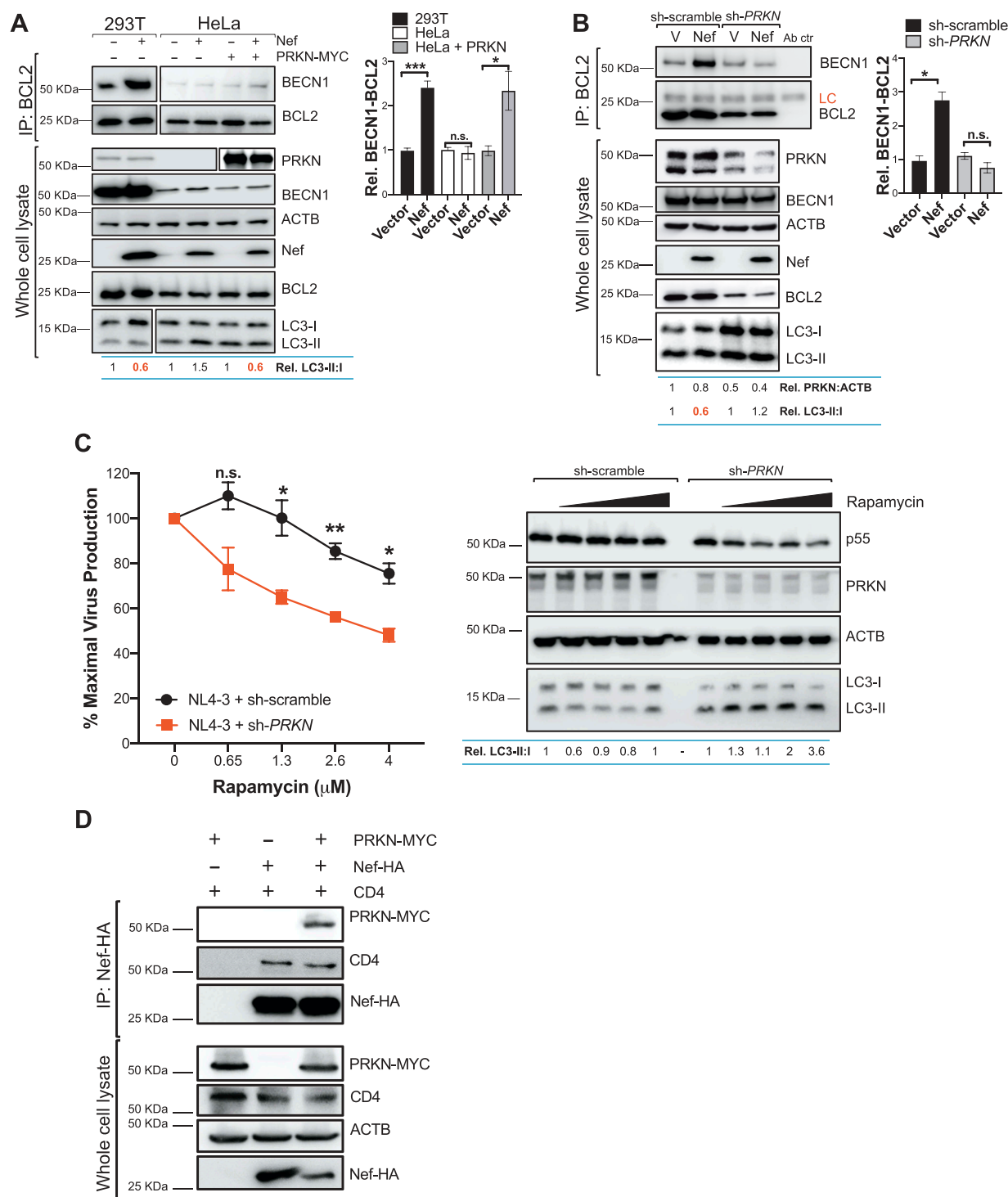
Figure 5. The Nef-enhanced association between BECN1 and BCL2 is PRKN-dependent. (A) HEK293T and HeLa cells were co-transfected with *BECN1*-Flag and either NL4-3 *nef* or an empty vector. In addition, HeLa cells were trans-complemented with *PRKN*-MYC. 48 h post-transfection, the cell lysates were immunoprecipitated for endogenous BCL2, and the pulldown fraction was examined for the presence of BECN1 and BCL2. The cell lysates were also subjected to western blot to assess the cellular levels of the proteins PRKN, BECN1, ACTB, Nef, BCL2, and LC3. The ratios of LC3-II over LC3-I relative to the empty vector are provided underneath the blots. Graph: Densitometric analyses were used to determine the relative levels of interaction between BECN1 and BCL2. Data represent the mean and SEM of 4 independent biological replicates. (B) HEK293T cells were depleted of PRKN by shRNA and subsequently co-transfected with *BECN1*-Flag and NL4-3 *nef* or an empty vector. Next, the cell lysates were analyzed for the BECN1-BCL2 interaction by immunoprecipitation and western blot. Similar to panel A, the relative PRKN expression levels normalized to ACTB as well as the ratios of LC3-II over LC3-I are provided underneath the blots. Graph: Densitometric analyses were used to determine the relative levels of interaction between BECN1 and BCL2. Data represent the mean and SEM of 4 independent biological replicates. (C) Left panel: HEK293T cells were depleted of PRKN by shRNA followed by transfection with the full-length proviral DNA of HIV-1 NL4-3. Cells were treated with the indicated concentrations (0–4 µM) of rapamycin for 12 h. The percentage of maximal virus production relative to the no-rapamycin treatment was then measured by the accumulation of HIV p24 in the culture supernatant. Data represent the mean and SEM of 3 independent biological replicates. Right panel: Cell lysates were also analyzed for Gag p55, PRKN, ACTB, and LC3. The ratios of LC3-II over LC3-I relative to the respective no-rapamycin treatments are provided underneath. (D) HEK293T cells were co-transfected with NL4-3 *nef*-HA and *PRKN*-MYC or an empty vector. Human CD4 was included as a positive control for Nef binding. 48 h later, cells were lysed and immunoprecipitated for HA. The affinity-isolated fraction was examined for the presence of PRKN-MYC, CD4 and Nef-HA. The cell lysates were also analyzed for the expression of PRKN-MYC, CD4, ACTB, and Nef-HA. V: vector. Rel: relative. Ab ctr: antibody control. LC: light chain. *: $p \leq 0.05$; ** $p \leq 0.01$; *** $p \leq 0.001$; n.s. not significant.

BECN1 and BCL2 and, in consequence, autophagy progression became restored, reflected by higher relative LC3-II:I ratios (Figure 5B; blots and graph). In agreement with these results, depletion of PRKN in rapamycin-stimulated cells caused a significant restriction in Gag levels and HIV-1 production (Figure 5C).

To explore how Nef uses this E3 ligase to block autophagy, we assessed the ability of Nef to interact with PRKN. For this, we performed co-immunoprecipitation assays in HEK293T cells co-expressing PRKN-MYC and NL4-3 Nef-HA. We included CD4 (cluster of differentiation 4) as a known interaction partner of Nef [105–112]. As expected, we found CD4 in the Nef pulldown fraction. Remarkably, PRKN also co-immunoprecipitated with Nef, indicating that these two proteins interact (Figure 5D). Thus, the association of Nef with PRKN is consistent with the requirement of this protein to facilitate the mono-ubiquitination of BCL2 and, in consequence, increase its association with BECN1, obstructing in turn autophagy initiation.

Nef increases BECN1-BCL2 binding on the endoplasmic reticulum

Besides its role in regulating autophagy, BCL2 plays an important role in eliciting pro-survival responses, and these two distinct functions depend on BCL2's subcellular localization. Whereas mitochondrial BCL2 is associated with anti-apoptotic responses, ER-bound BCL2 is involved in the regulation of autophagy through its association with BECN1 [13,93–95,97,113–119]. However, PRKN primarily localizes in the mitochondria [120]. To investigate if Nef increases BCL2 ubiquitination and association with BECN1 in the mitochondria or the ER, we monitored how NL4-3 Nef affects BCL2's PTMs in each compartment, and their effect on BECN1 binding. To address this, we transfected HEK293T cells with GFP-tagged BCL2 constructs fused with ER CYB5A (cytochrome B5) or mitochondrial MAOB (monoamine oxidase B) target sequences to drive their distinct subcellular localization [114]. Consistent with the data in Figure 4C, we found that Nef enhanced the ubiquitination and phosphorylation levels of the total GFP-BCL2 control – which can associate with both the ER and the mitochondria – as well as the ER-BCL2 and Mit-BCL2 isoforms (Figure 6A). However, the effect of Nef on BECN1-BCL2 binding differed when we analyzed the subcellular variants. Whereas the presence of Nef caused an overall increase in BECN1-BCL2 binding for total GFP-BCL2 and more strikingly for ER-BCL2, Nef did not enhance the interaction between BECN1 and Mit-BCL2 (Figure 6A; graphs). This result is consistent with the fact that the ER-bound variant is the main isoform involved in the regulation of autophagy [93,94]. Immunofluorescence images of HEK293T cells co-expressing ER-BCL2, BECN1-Flag, and either HA-GST (as an irrelevant protein) or NL4-3 Nef-HA supported this mechanism. As expected, we found colocalization between BECN1 and ER-bound BCL2 in the presence of HA-GST. However, Nef significantly increased the colocalization of BECN1 and ER-BCL2 (Figure 6B). Therefore, these findings suggest a model in which Nef enhances PRKN-mediated ubiquitination of BCL2 on the ER, consequently

arresting autophagy through the sequestration of BECN1 (Figure 6C).

The Nef-mediated enhancement in the BECN1-BCL2 interaction also affects the functionality of the class III PtdIns3K complex II

Besides causing considerable retention of LC3-I, Nef also increased the overall levels of LC3-II, particularly in the presence of total GFP-BCL2 and ER-associated GFP-BCL2 (Figure 6A; bottom blots). This phenomenon has already been described by others and reflects an additional mechanism by which Nef blocks autophagy at the maturation level by preventing the fusion between autophagosomes and lysosomes [38,49]. In addition to phagophore nucleation, BECN1 also participates in the maturation stages of autophagy by being part of the class III PtdIns3K complex II [121,122]. Therefore, to investigate whether the Nef-mediated enrichment in BECN1-BCL2 also affects the formation of class III PtdIns3K complex II, we explored changes in the interaction patterns between BECN1 and UVRAG, a molecule that is exclusively found in class III PtdIns3K complex II [121]. For this, we immunoprecipitated UVRAG from HEK293T cells co-expressing BECN1-Flag and either an empty vector, ER-BCL2, NL4-3 Nef, or both (ER-BCL2 and Nef). We then analyzed the pulldown fraction for UVRAG and BECN1. Overexpression of ER-BCL2 caused a significant reduction in BECN1-UVRAG binding, suggesting that the BCL2-mediated sequestration of BECN1 affected both PtdIns3K complexes. Since Nef increases the association between ER-BCL2 and BECN1, we found a similar phenotype in cells expressing Nef. Accordingly, co-expression of ER-BCL2 and Nef reduced even further binding between UVRAG and BECN1 (Figure 7A; blots and graph). Remarkably, either through overexpression of ER-BCL2, Nef or both, we detected marked retention in LC3-I, accompanied by accumulation of LC3-II (Figure 7A; blots), confirming that by increasing the interaction between BCL2 and BECN1, autophagy is not only arrested at the initiation stages but also in the maturation level.

Previous studies have pointed to a region in the N-terminus of Nef as being responsible for blocking autophagy maturation. Specifically, amino acids $D_{36}LEK_{39}$ in NL4-3 Nef mimic sequences used by RUBCN, an autophagy inhibitor that affects the functionality of class III PtdIns3K complex II [50]. To explore if Nef also uses this domain to intersect with the initiation stages of autophagy, we introduced alanine substitutions in this region of Nef (Nef$^{A36-A39}$), and examined autophagosome formation by flow cytometry and western blotting, as explained above. Remarkably, the Nef$^{A36-A39}$ mutant exhibited a different western blot migration pattern compared to wild type NL4-3 Nef, although their expression levels remained similar (Figure 7C,D). Sequencing verification analyses indicated that our mutagenesis protocol did not incorporate additional nucleotide changes in the expression vector or the Nef coding region. Therefore, we concluded that the hydrophobic residues introduced in the RUBCN-like motif were responsible for this phenotype. Despite this unusual migration profile,
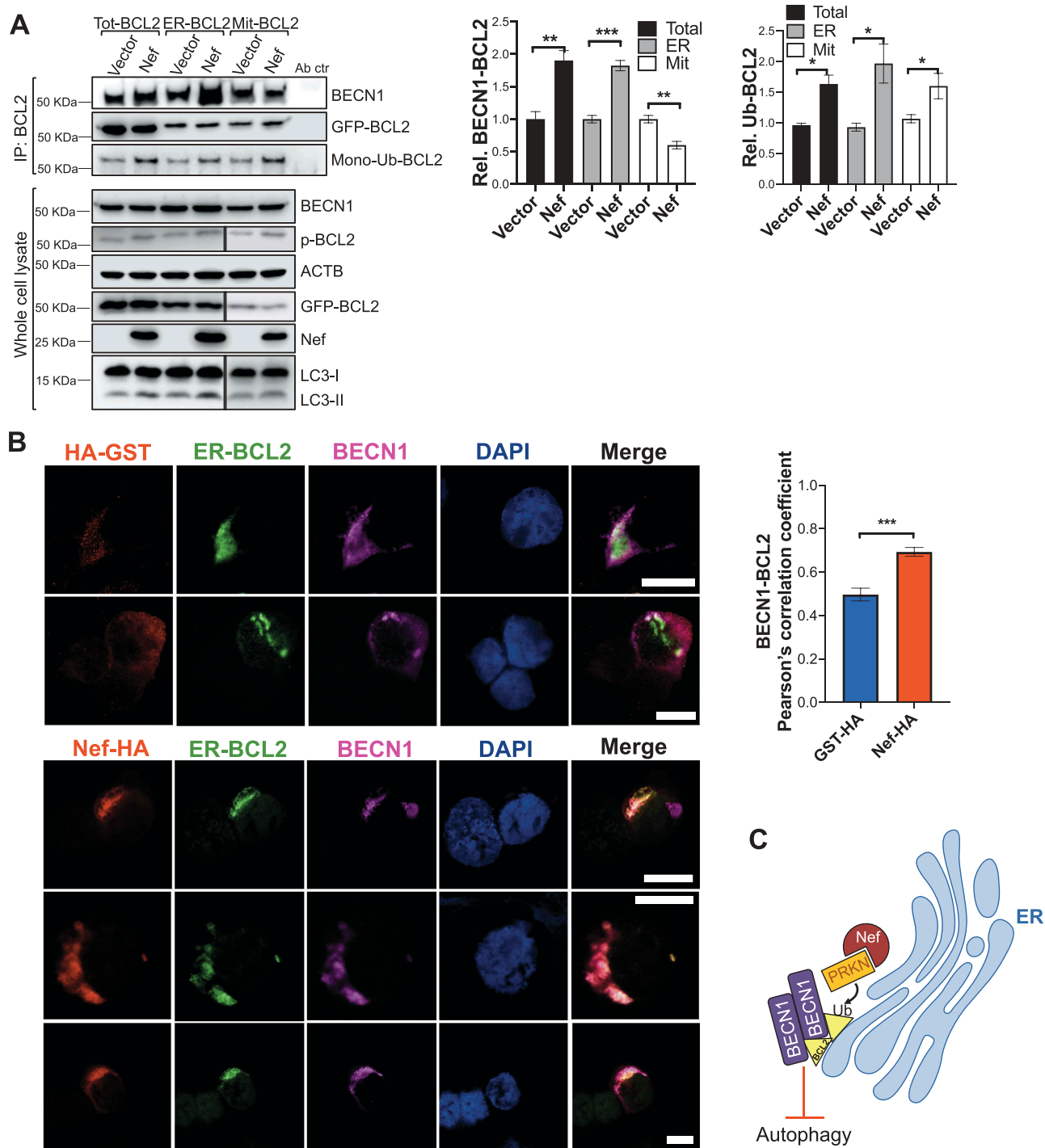
Figure 6. Nef promotes BECN1-BCL2 binding in the ER. (A) HEK293T cells were co-transfected with *BECN1*-Flag and Tot-GFP-*BCL2* (total BCL2), ER-GFP-*BCL2* (Endoplasmic Reticulum-associated BCL2) or Mit-GFP-*BCL2* (Mitochondrial BCL2). In addition, cells were transfected with NL4-3 *nef* or an empty vector. 48 h later, the cell lysates were immunoprecipitated for BCL2. The pulldown fraction was examined for the presence of BECN1, GFP-BCL2 and Ub-BCL2. The cell lysates were also analyzed by western blot to assess the cellular levels of BECN1, p-BCL2, ACTB, GFP-BCL2, Nef, and LC3. Graphs: Densitometric analyses were used to determine the relative interaction between BECN1 and BCL2 and the relative levels of ubiquitinated BCL2. Data represent the mean and SEM of 5 independent biological replicates. (B) HEK293T cells were co-transfected with *BECN1*-Flag, ER-GFP-*BCL2* and either *GST*-HA or NL4-3 *nef*-HA. 48 h later, cells were stained for HA (DyLight-550; red), ER-GFP-BCL2 (green), BECN1-Flag (Alexa Fluor 633; magenta) and nuclei (DAPI; blue). Merge of HA, ER-GFP-BCL2 and BECN1-Flag is provided. The Pearson's correlation coefficient for the colocalization of BECN1 and BCL2 is provided in a graph from 15 independent events for each experimental condition. (C) Proposed mechanism by which Nef arrests autophagy initiation. Rel: relative. Ab ctr: antibody control. *: $p \leq 0.05$; **: $p \leq 0.01$; ***: $p \leq 0.001$. White scale bar: 10 μm.

Nef[A36-A39] retained the ability to block autophagosome formation, depicted by significantly lower membrane-associated EGFP-LC3B than the vector control (Figure 7B). Accordingly,

Nef[A36-A39] caused substantial retention in LC3-I, even greater than wild type Nef (Figure 7C), indicating that this domain is dispensable to block autophagy initiation. In fact, Nef[A36-A39]
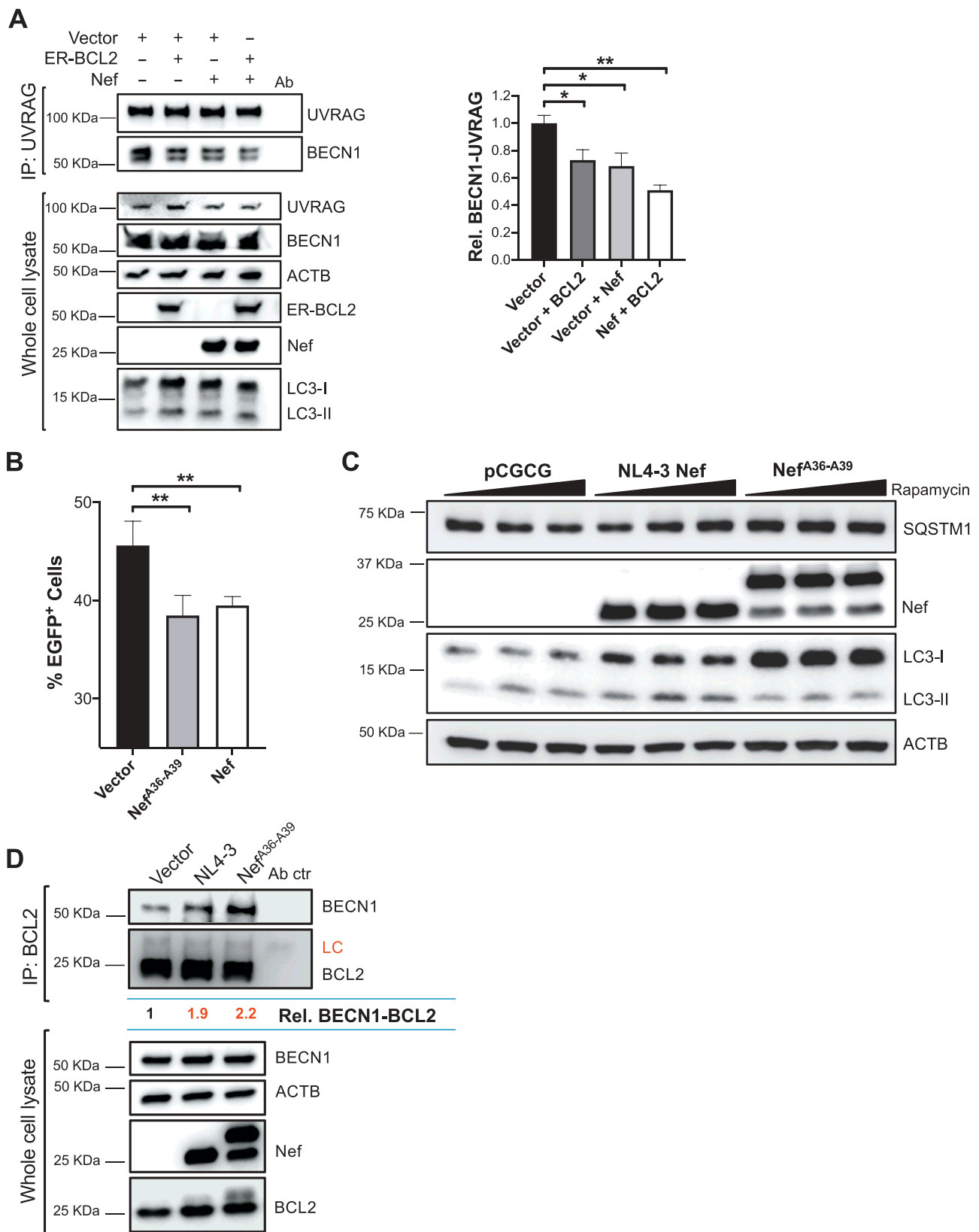
Figure 7. The Nef-enhanced sequestration of BECN1 by BCL2 also affects autophagy maturation. (A) HEK293T cells were co-transfected with *BECN1*-Flag and an empty vector, NL4-3 *nef* and/or ER-GFP-*BCL2*. 48 h later, cells were immunoprecipitated for UVRAG and the pulldown fraction was analyzed for the presence of UVRAG and BECN1-Flag. The cell lysates were also examined for UVRAG, BECN1, ACTB, ER-GFP-BCL2, Nef, and LC3. Graph: Densitometric analyses were used to determine the relative interaction between BECN1 and UVRAG. Data represent the mean and SEM of 3 independent biological replicates. (B-D) Nef[A36-A39] was examined for its ability to block autophagosome formation by flow cytometry through the accumulation of autophagosome-associated EGFP-LC3B (B), its ability to prevent the lipidation of LC3 by western blot (C), and its ability to enhance the BECN1-BCL2 interaction by co-immunoprecipitation (D). Assays were carried out in HEK293T cells, as detailed previously. pCGCG-EGFP or pcDNA5 were used as vector controls, NL4-3 *nef* or NL4-3 *nef*-HA were used to express HIV-1 Nef. Data correspond to the mean and SEM of 4 independent experiments. Rel: relative. Ab ctr: antibody control. LC: light chain. *: $p \leq 0.05$; **: $p \leq 0.01$.

still increased the association between BECN1 and BCL2 (Figure 7D). By contrast, expression of this mutant significantly reduced the accumulation of LC3-II (Figure 7C), which is consistent with previous reports showing that this motif is necessary to prevent autophagy maturation [50]. Therefore, our findings indicate that Nef uses two different mechanisms on separate domains to repress both autophagy initiation and maturation.

The ability of Nef to block autophagy is mainly observed in HIV-1/SIV$_{cpz}$

Despite the sequence variability in *nef* among the primate lentiviruses, its functional activities are usually conserved, including downregulation of CD4, CD28, SERINC3, SERINC5, and major histocompatibility complexes [56,123,124]. To investigate if this is also the case for its ability to arrest autophagy, we analyzed a set of 23 *nef* genes from primary isolates of pandemic HIV-1 as well as representative HIV-2 variants and the simian precursors of both of these human viruses (SIV$_{cpz}$ and SIV$_{smm}$). Specifically, we assessed their ability to block autophagy by examining the conversion of LC3-I into LC3-II and SQSTM1 levels under conditions of rapamycin stimulation. As controls, we used the empty pCGCG-EGFP vector and NL4-3 Nef (Figure 8A; representative results for one Nef allele). We performed these experiments 3 independent times to calculate the relative LC3-II:I ratios as well as any statistical differences with the vector control. We found that the ability of Nef to block autophagy was present in the HIV-1/SIV$_{cpz}$ lineage (Figure 8B,D; red arrows and colored squares), while this activity was largely missing in the HIV-2/SIV$_{smm}$ panel (Figure 8C,D), and we confirmed these observations by flow cytometric analysis of autophagosome-associated EGFP-LC3B (not shown).

Primate lentiviruses exhibit high plasticity in the use of their accessory proteins to overcome restriction factors. This plasticity is particularly evident for BST2. Whereas HIV-1 primarily uses Vpu as a BST2 countermeasure, HIV-2 uses Env, and the majority of SIVs use Nef [80,125–131]. Therefore, it would not be surprising if HIV-1/SIV$_{cpz}$ use Nef as their primary autophagy antagonist, while members of the HIV-2/SIV$_{smm}$ lineage devote a different protein for this task. To test this hypothesis, we transfected HEK293T cells with the full-length proviral DNA of SIV$_{mac}$239, a virus that originated after the cross-species transmission of SIV$_{smm}$ from sooty mangabeys to rhesus macaques. We also included SIV$_{mac}$239 mutants harboring deletions in *nef* and *env* as well as the molecular clone of SIV Δ*nef*P, a virus that regained virulence after serial passage in rhesus macaques by accumulating compensatory mutations in gp41 [82,132]. As controls, we included an empty retroviral vector, and the proviral DNA of wild type NL4-3 and NL4-3 Δ*nef*. Compared to HIV-1 NL4-3, none of the SIV$_{mac}$239 clones tested were able to overcome autophagy, since they did not affect the conversion of LC3-I into LC3-II, and the relative levels of SQSTM1 were considerably lower than NL4-3, reflecting normal autophagy flux (Figure S6A; right panel). Accordingly, the relative LC3-II:I ratios were significantly higher than NL4-3. Consistent

with these findings, when we exposed HEK293T cells transfected with SIV$_{mac}$239 or SIV$_{mac}$239 Δ*nef* to rapamycin stimulation, we observed a similar dramatic reduction in particle release, indicating that autophagy poses a hurdle for SIV (Figure S6B).

Discussion

Autophagy is a conserved, highly regulated system by which eukaryotic cells eliminate cytoplasmic targets such as damaged organelles and misfolded proteins, but also viral components, serving as a defense mechanism against viruses. Thus, the antiviral properties that autophagy exerts provide an opportunity to manipulate this cellular pathway to help contain viral infections [1,2,18,27,30,31,133,134]. However, many viruses have evolved to circumvent and/or usurp autophagy to ensure their propagation [2,27,33–35]. In consequence, there is a critical need to elucidate the interplay between autophagy and virus pathogens, such as HIV, before we can consider the pharmacological manipulation of this cascade as an antiviral therapeutic approach.

Several studies have investigated the interactions between HIV and the autophagy machinery with mixed results, and these differences become particularly evident in a cell-type-specific manner [38,39,47–49,51-55,67]. In an effort to bring consensus, we examined the basal autophagy status of different HIV target cells, as well as their sensitivity to diverse autophagy stimuli, to better understand the HIV-autophagy interplay in each cellular environment. We found that each cell type exhibits differences in their basal autophagy levels as well as in the threshold to induce this survival cascade, and thus, distinct cell types react differently to external stressors known to trigger autophagy (i.e., cytoplasmic DNA, RNA as well as transfection reagents) [1,2,70,135,136]. By considering all these aspects, plus measuring autophagy status through relative ratios of LC3-II:I, we have been able to compare the effect of HIV on autophagy in different cellular contexts. Our results demonstrate that HEK293T cells, macrophages and CD4$^+$ T cells respond to HIV by triggering autophagy, causing a reduction in HIV Gag levels and virion production. However, HIV has evolved to circumvent autophagy antiviral effects by hampering the progression of this pathway through the viral protein Nef. This phenomenon is evidenced by the fact that infections with *nef*-deleted viruses do not influence autophagy flux, but the presence of Nef causes a defect in the conversion of LC3-I into LC3-II – a hallmark for autophagy activation – in all cell types tested.

Previous studies have indicated a role for Nef in blocking autophagy in macrophages [38,49], and they reported that Nef achieves this by two different mechanisms. Whereas one report stated that HIV activates autophagy early during infection to aid in uncoating and that the virus uses Nef to block this pathway at later stages by preventing the formation of autolysosomes [38], a later publication described that Nef halts autophagy through the cytoplasmic sequestration of TFEB [49]. More recently, structural studies in the Hurley lab revealed that Nef harbors sequences in its N-terminal domain that mimic the class III PtdIns3K complex II-binding domain (PIKBD) of RUBCN, an inhibitor of BECN1.
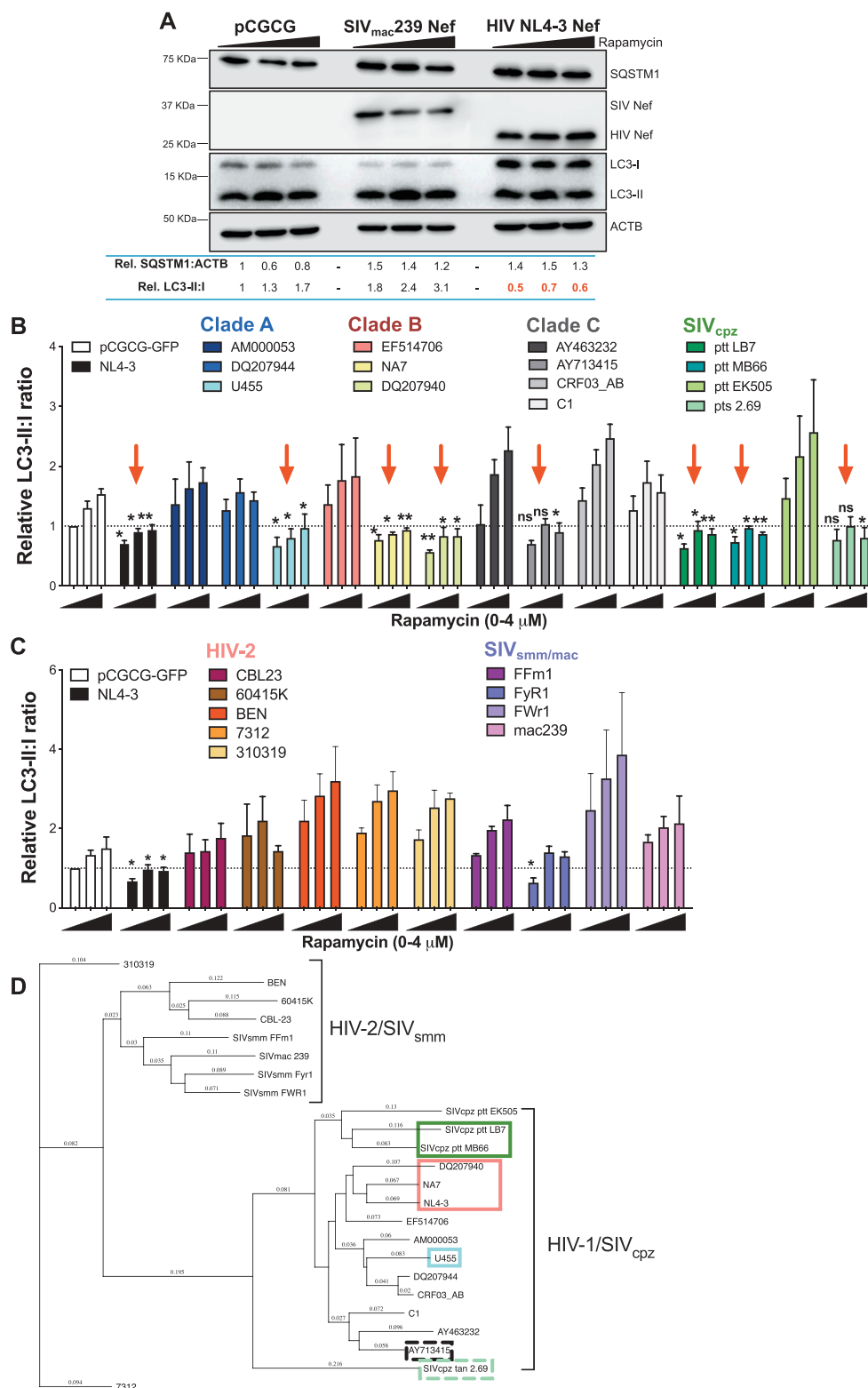
Figure 8. Nef's ability to inhibit autophagy is mainly observed in HIV-1/SIV$_{cpz}$. (A) Representative data of the analyses of the anti-autophagic properties of lentiviral Nef proteins. HEK293T cells were transfected with NL4-3 *nef*, an empty vector and SIV$_{mac}$239 *nef*. 48 h later, cells were exposed for 4 h to increasing concentrations of rapamycin (0–4 μM). Next, cells were analyzed by western blot for the levels of SQSTM1, Nef, LC3, and ACTB. Densitometric analyses were performed to determine the levels of SQSTM1:ACTB and the ratio of LC3-II over LC3-I relative to the empty vector control under no rapamycin treatment. (B, C) Data correspond to the mean and SEM of the relative LC3-II:I ratios from 3 independent biological replicates of different lentiviral *nef* alleles of the HIV-1/SIV$_{cpz}$ lineage (B) and HIV-2/SIV$_{smm}$ lineage (C). (D) The amino acid sequence of Nef from the different lentiviral species was compared and clustered in a cladogram where the relative evolutionary distance between each variant is shown. Color-coded squares are used to identify species in which Nef is able to inhibit autophagy (solid line) or exhibit partial activity (dashed line). *: $p \leq 0.05$; **: $p \leq 0.01$; n.s. not significant. Red arrows indicate Nef alleles active against autophagy.

The findings in that study support the notion that Nef interacts with BECN1 through this PIKBD-like domain, blocking class III PtdIns3K complex II and, in turn, autolysosome formation [50,137]. In line with these observations, we also found that cells expressing Nef frequently display high levels of SQSTM1 and LC3-II, reflecting a block in autophagy maturation. Consistent with this, our data show that Nef significantly reduces the association between UVRAG and BECN1 in class III PtdIns3K complex II, which would consequently impair autophagosome-lysosome fusion. However, our studies revealed that Nef additionally prevents autophagy initiation through a previously unrecognized mechanism and that this effect is independent on Nef's PIKBD-like domain, indicating that Nef uses distinct protein surfaces to obstruct autophagy initiation and maturation. Specifically, our data demonstrate that Nef enhances BECN1 association with BCL2, preventing the formation of phagophore structures early in the autophagy cascade [10,103,138]. Upon autophagy activation, BECN1 dissociates from GLIPR2/GAPR-1 (GLI pathogenesis related 2) in Golgi and translocates to the ER to facilitate the nucleation of phagophores [85]. BECN1 achieves this by forming the class III PtdIns3K complex I, a multimolecular complex that mediates the synthesis of PtdIns3P [95–97]. PtdIns3P is an essential element for phagophore biogenesis, the lipidation of LC3, and thus, autophagy initiation. Remarkably, when bound to the mono-ubiquitinated form of BCL2, BECN1 is unable to promote the formation of such enzymatic complex. Our studies demonstrate that Nef intersects with these early stages of autophagy by increasing the mono-ubiquitination of ER-bound BCL2 through PRKN. Binding assays and imaging studies showing a significant increase in the colocalization of ER-BCL2 and BECN1 in the presence of Nef support this notion. PRKN plays an important role in mitochondrial quality control [102], but also regulates autophagy through BCL2 mono-ubiquitination [100]. The role of PRKN in the Nef-mediated inhibition of autophagy is unprecedented and verified in our binding assays and experiments in PRKN⁺ (HEK293T) and PRKN⁻ (HeLa) cells. In fact, when PRKN is provided in trans to PRKN⁻ cells, Nef enhances the association between BECN1 and BCL2, which is accompanied by an impairment in the transition of LC3-I to LC3-II. Finally, the selective depletion of PRKN in HEK293T cells causes a loss-of-function phenotype in which Nef cannot enhance the BECN1-BCL2 interaction, rendering HIV susceptible to autophagy restriction.

The Nef-mediated enrichment in the interaction between BECN1 and BCL2 consequently obstructs the lipidation of LC3, which is particularly evidenced in the presence of lysosomal inhibitors. Under these conditions, the overall levels of LC3-II increase due to a defect in lysosomal function. However, we still observed the retention in LC3-I in cells expressing Nef, supporting a defect in the LC3-I-to-LC3-II conversion. Remarkably, only when autophagy maturation is halted, Gag levels are restored, suggesting that Gag is an autophagy target. While our findings indicate that the accumulation of LC3-I in the presence of Nef is a consequence of blocking early autophagy steps, an increase in LC3-I might also reflect indirect effects of Nef on the expression of LC3B. To rule this out, we monitored the transcription levels of this gene, which is regulated by several transcription factors, among them TFEB [89]. As anticipated, no increase in the expression of LC3B was detected. On the contrary, Nef

downmodulates its transcription. Although these results may be in line with Campbell et al. observations in macrophages, where they reported that Nef blocks autophagy by sequestering TFEB in the cytoplasm [49], our transcriptional assays also examined fluctuations in the expression levels of another TFEB target: ATG16L1 [89]. Unlike the effects of Nef on LC3B, we found no significant changes in ATG16L1 expression. Therefore, these results confirm that the accumulation of LC3-I observed in the presence of Nef is not the result of the upregulation of this gene and that, in our system, Nef likely blocks autophagy in a TFEB-independent manner.

Nef is well-known for its ability to facilitate immune evasion through multiple mechanisms, and most of these activities are conserved in the primate lentiviruses [65,123,124,139]. Unlike these well-preserved functions, our screens of primary Nef alleles from HIVs and SIVs indicate that the ability to counteract autophagy restriction may be mainly found in the HIV-1/SIV_cpz lineage. Specifically, pandemic HIV-1 clade B Nef alleles are potent autophagy antagonists. Although clade C isolates are most prevalent due to their high incidence in Africa and Asia, isolates belonging to clade B are ubiquitously found around the globe, suggesting that autophagy antagonism may be influencing the spread and pathogenesis of HIV-1. Future studies will test this hypothesis by surveying Nef alleles of HIV-1 primary isolates obtained from acute infection (transmitted/founder viruses), and assessing whether their capacity to overcome the autophagy block correlates with their increased transmission, infectivity, and pathogenesis.

The fact that some Nef alleles from primary isolates are poor autophagy antagonists suggests that these viruses are either unable to antagonize the autophagy block or that they have evolved other genes for this purpose. To test this hypothesis, we tested SIV_mac239, a virus we have extensively studied due to its plasticity to overcome restriction factors [80–83], for its ability to antagonize autophagy. Unlike HIV-1 NL4-3, SIV_mac239 failed at impairing autophagy flux, and thus, was highly susceptible to autophagy restriction, indicating that SIV_mac239 has not evolved alternative mechanisms to counteract the autophagy block. However, since species-specific differences have dictated the adaptation and evolution of the primate lentiviruses in their respective hosts, we cannot fully rule out that the inability of SIV_mac239 to counteract autophagy in the context of HEK293T cells (of human origin) is due to species-specific differences in the autophagy proteins targeted by Nef between humans and non-human primates. We are currently investigating this potential scenario.

In summary, here we have demonstrated that HIV-1 is susceptible to autophagy restriction, but the virus uses the Nef accessory protein to circumvent this barrier. The role of Nef in blocking autophagy progression has already been reported by other studies, particularly in macrophages. Consistent with these reports, we found that Nef is a potent autophagy antagonist that interferes with the maturation step of this pathway. However, our studies indicate that Nef exhibits an additional mechanism to halt autophagy at the initiation stages. Specifically, Nef enhances the association between the autophagy protein BECN1 and its inhibitor BCL2 by

enhancing BCL2 mono-ubiquitination in a PRKN-dependent manner. Because BECN1 is necessary for the formation of autophagosome structures, its sequestration by BCL2 causes defects in autophagosome formation and, consequently, in maturation, allowing in turn efficient virion assembly and release. HIV Nef is a well-known immune evasion factor through the downregulation of the immune receptors CD4, C28 and major histocompatibility complexes as well as the restriction factors SERINC3 and SERINC5 [56–65]. Therefore, in addition to its already known functional activities, here we show that Nef antagonizes the antiviral effects of autophagy through a previously unrecognized mechanism that affects autophagy at different stages of the pathway.

Materials and methods

Plasmid DNA constructs

(i) *HIV-1 proviral clones.* The following full-length proviral constructs were obtained through the NIH AIDS Reagent Program, Division of AIDS, NIAID, NIH, from Drs. Malcolm Martin, Klaus Strebel, Robert Siliciano, Olivier Schwartz, and Nathaniel Landau, respectively [140–143]. Specifically, full-length constructs for wild type HIV-1 NL4-3 (pNL4-3, 114), NL4-3 Δvpu (pNLU35, 968), NL4-3 Δenv (pNL4-3 ΔEnv EGFP, 1110), NL4-3 Δnef (pNL4-3 ΔNef, 12755), NL4-3 ΔenvΔnef (pNL4-3.HSA.R$^+$E$^-$, 3420), and NL4-3 Δvpr (pNL4-3.HSA.R$^-$, 3417). HIV-1 NL4-3 viruses based on these plasmids were generated by transient transfection in HEK293T cells, as previously described [80,81,144].

(ii) *SIV$_{mac}$ 239 proviral clones.* Full-length SIV$_{mac}$ 239 proviral DNA as well as mutants of this molecular clone, Δnef, ΔenvΔnef and ΔnefP, were a gift from Dr. David T. Evans (University of Wisconsin, Madison, WI). These constructs were assembled from p239SpSp5′, pSP72-239-3′, pSP72-239-3′Δnef, pSP72-239-3′Δenv and p3′ITMΔnefΔUS138, as previously described [80,81,132,145,146].

(iii) *VSV-G construct.* The plasmid for the expression of the Indiana variant of the vesicular stomatitis virus (VSV) glycoprotein was a gift from Dr. David T. Evans (University of Wisconsin, Madison, WI).

(iv) *HIV and SIV Nef expression vectors.* The expression vector pCGCG (a gift from Dr. Jacek Skowronski [Case Western Reserve University, Cleveland, OH]), which harbors EGFP from an internal ribosomal entry site, was used to clone different Nef alleles using the XbaI and MluI unique restriction sites. The following Nef alleles were cloned into this vector: HIV-1 NL4-3 Nef, HIV-1 CRF03_AB Nef, HIV-1 C1 Nef, HIV-1 U455 Nef, HIV-1 AY713415 Nef, HIV-1 AY463232 Nef, HIV-1 AM000053 Nef, HIV-1 DQ207940 Nef, HIV-1 DQ207944, HIV-1 EF514706, HIV-1 NA7 Nef, HIV-2 CBL-23 Nef, HIV-2 60415K Nef, HIV-2 BEN Nef, HIV-2 7312 Nef, HIV-2 310319 Nef, SIV$_{cpz}$ ptt LB7 Nef, SIV$_{cpz}$ ptt MB66 Nef, SIV$_{cpz}$ ptt EK505 Nef, SIV$_{cpz}$ pts 2.69

Nef, SIV$_{sm}$ FFm1 Nef, SIV$_{sm}$ FyR1 Nef, SIV$_{sm}$ FwR1 Nef, and SIV$_{mac}$ 239 Nef [80,124,130,147,148]. In addition, an HA-tagged version of NL4-3 Nef was obtained from Addgene: pCI-NL4-3 Nef-HA-WT (24162, Dr. Warner Greene's lab). NL4-3 Nef$^{A36-A39}$ was generated by site-directed mutagenesis and cloned into pCGCG.

(v) *Plasmids coding for autophagy proteins.* The following constructs were obtained through Addgene: pEMD-C1-GFP-BCL2 fusion genes (GFP-BCL2, 17999; GFP-BCL2-Cb5, 18000; and GFP-BCL2-Maob, 18001; all obtained from Dr. Clark Distelhorst's lab), pRK5-PRKN-MYC (7612, Dr. David Root's lab), pC3-EGFP-LC3B (11546, Dr. Karla Kirkegaard's lab), pMX-GFP-ZFYVE1 (38269, Dr. Noboru Mizushima's lab), and pcDNA4-BECN1-Flag (24388, Dr. Qing Zhong's lab). The protein GST was HA-tagged and cloned into pcDNA5 (ThermoFisher Scientific, V601020), as previously described [83].

Transfections

6 x 10^5 HEK293T (American Type Culture Collection [ATCC], CRL-11268) and HeLa (NIH AIDS Reagent Program, Division of AIDS, NIAID, NIH from Dr. Richard Axel; 153) cells were transfected using GenJet *in vitro* DNA transfection reagent (SignaGen Laboratories, SL100488), following the manufacturer's suggestions, including total DNA, dish size, incubation time, and the ratio of GenJet:DNA for optimal transfection efficiency. Cell viability was monitored for every transfection to evaluate if the expression of the above-described constructs could cause cellular toxicity or damage. No evidence of toxicity was observed. If viability was below 85%, cells were considered unsuitable for further analyses. Viabilities were usually above 90%.

Infections

(i) *Jurkat cells.* One million Jurkat CD4$^+$ T cells (ATCC, TIB-152) were infected with 100 ng of p24 equivalents of HIV-1 NL4-3 or NL4-3 Δnef for 3 h at 37°C. Cells were then washed and re-suspended in 5 mL of R10: RPMI medium (ThermoFisher Scientific, 11875–119) supplemented with 10% of fetal bovine serum (ThermoFisher Scientific, 26140–079). Cell samples were collected at 6, 24, 48, 60, 72, 84, 96, 108, 120, and 132 h post-infection for their analysis by western blot.

(ii) *CD4$^+$ T cells from PBMCs.* One million naïve CD4$^+$ T cells isolated from PBMCs (Zenbio, Inc., SER-PBCD4 TH-N-F) were activated using Dynabeads coated with anti-CD3 and anti-CD28 antibodies (ThermoFisher Scientific, 111.31D). Cells were also expanded using IL2 (interleukin 2; 30 IU/mL; NIH AIDS Reagent Program, Division of AIDS, NIAID, NIH; 136) for 3 d. Next, cells were infected with 100 ng of p24 equivalents of HIV-1 NL4-3 or NL4-3 Δnef

for 3 h at 37°C. Cells were then washed and re-suspended in 3 mL of R10 medium. Cell lysates were collected at 6, 72, and 120 h post-infection for their analysis by western blotting.

(iii) *THP1-derived macrophages*. One million THP-1 monocytes (ATCC, TIB-202) were differentiated into macrophages after stimulation with 200 nM of PMA (phorbol 12-myristate 13-acetate; Sigma-Aldrich, P1585) for 3 d. Differentiation to a macrophage phenotype was confirmed by microscopy after the PMA treatment. Next, macrophages were infected with 100 ng of p24 equivalents of VSV-G pseudotyped HIV-1 NL4-3 Δ*env* or NL4-3 Δ*env*Δ*nef* for 3 h at 37°C. Cells were washed and re-suspended in 3 mL of R10 medium. Cell lysates were collected at 6, 72 and 120 h post-infection for their analysis by western blotting.

Virus release assays

6 x 10⁵ HEK293T cells were transfected with 2,000 ng of full-length proviral DNA of HIV-1 NL4-3, NL4-3 Δ*nef*, SIV$_{mac}$ 239, or SIV$_{mac}$ 239 Δ*nef*. For the trans-complementation studies, transfections with *nef*-deleted proviruses also included pCGCG-NL4-3 Nef or the empty vector pCGCG. 24 h post-transfection, the cell medium was replaced, and rapamycin (Sigma-Aldrich, R8781) was added at different concentrations (0–4 μM). In the competition assays between rapamycin and 3-methyladenine (3-MA; Sigma-Aldrich, M9281), this compound was added at 3 mM 8 h after rapamycin stimulation. In the lysosomal inhibition assays, chloroquine (Sigma-Aldrich, C6628-256) was added at 60 μM together with rapamycin. In the experiments with the BCL2 inhibitor GX15-070 (AdooQ, A10665), this compound was added along with rapamycin at 3 μM, which corresponds to its IC$_{50}$. 48 h post-transfection, the culture supernatants were collected and analyzed by p24 or p27 antigen-capture ELISA (Advanced Biolabs, 5421 and 5436), as previously described [80–83,144]. In the case of virus release assays in Jurkat cells, 10⁶ Jurkat cells were infected with 100 ng of p24 equivalents of HIV-1 NL4-3 or NL4-3 Δ*nef* for 3 h at 37°C. Cells were then washed and re-suspended in 5 mL of R10 medium. 24 h later, cells were washed and aliquoted into 24-well plates at 150,000 cells per well. Cells were stimulated with rapamycin (0–6.5 μM) for 12 h. Virion release was determined as explained above. In addition, cells were washed, lysed, and harvested for their analysis by western blotting.

Western blotting

Cells, including HEK293T, HeLa, Jurkat, THP-1, as well as primary CD4⁺ T cells were harvested in lysis IP buffer (ThermoFisher Scientific, 87787) complemented with protease inhibitors (Roche, 04693116001) and phosphatase inhibitor cocktails 2 and 3 (Sigma-Aldrich, P5726 and P0044). Cell lysates were incubated on ice for 1 h. Samples were then centrifuged at 16,000 x *g* for 8 min. The supernatant was collected, mixed with 2x SDS sample buffer (Sigma-Aldrich, S3401) and boiled for 5 min. Proteins were then separated by electrophoresis on SDS-PAGE polyacrylamide gels (8-12%)

and transferred to a polyvinylidene difluoride (PVDF) membrane (BioRad, 1620177) using a Trans-Blot SD transfer cell (BioRad, 1703940). After blocking the membranes for 1 h in blocking buffer (BioRad, 1706404) at room temperature, we proceeded with the incubation with primary antibodies overnight at 4°C (antibody sources and dilutions are detailed in Table 1). Next, membranes were washed 3 times in PBS-tween (Sigma-Aldrich, P3563) for 15 min at room temperature before being probed for 1 h with the secondary antibody solution at a 1:2,000 dilution. Three different secondary antibodies were used, all conjugated with horseradish peroxidase: goat anti-mouse-HRP, goat anti-rabbit-HRP and donkey anti-rabbit-HRP (Table 1). After the incubation with the secondary antibodies, the membranes were washed 3 additional times in PBS-tween, developed using SuperSignal West Femto maximum sensitivity substrate (Pierce, 34095), and visualized using a Li-Cor Odyssey Fc Imager 2800 (Li-Cor, Lincoln, NE).

Knockdown assays

esiRNA was used to knockdown human *BECN1*, while *PRKN* was depleted using shRNA.

The esiRNA oligos were obtained from Sigma-Aldrich (EHU061741), and harbored the following sequences to silence *BECN1*: GGCTGAGAGACTGGATCAGGAGGAAGCTCAGTAT CAGAGAGAATACAGTGAATTTAAACGACAGCAGCTGGAG-CTGGATGATGAGCTGAAGAGTGTTGAAAACCAGATGCGT-TATGCCCAGACGCAGCTGGATAAGCTGAAGAAAACCAAC-GTCTTTAATGCAACCTTCCACATCTGGCACAGTGGACAG-TTTGGCACAATCAATAACTTCAGGCTGGGTCGCCTGCCC-AGTGTTCCCGTGGAATGGAATGAGATTAATGCTGCTTGG-GGCCAGACTGTGTTGCTGCTCCATGCTCTGGCCAATAAG-ATGGGTCTGAAATTTCAGAGATACCGACTTGTTCCTTAC-GGAAACCATTCATATCTGGAGTCTCTGACAGACAAATCT-AAGGAGCTGCCGTTATACTGTTCTGGGGGGTTGCGGTTT-TTCTGGGACAACAAGTTTGACCATGCAATGGTGGCTTTC-CTGGACTGTGTGCAG.

BECN1 depletion was achieved by transient transfection of the esiRNAs in 6 × 10⁵ HEK293T cells, using Lipofectamine 3000 *in vitro* transfection reagent following the manufacturer's instructions (ThermoFisher Scientific, L3000015). Knockdown was verified by western blot 3–5 d post-transfection.

Human *PRKN* was silenced using the following Dharmacon shRNA constructs: *TRCN0000000281, TRCN0000000282, TRCN 0000000283, TRCN0000000284, TRCN0000000285*. Protein depletion was achieved by transient transfection of a combination of different shRNAs, following the same transfection protocols described above. PRKN knockdown was verified by western blot 3–5 d post-transfection.

RT-qPCR assays

(i) *RNA extraction and cDNA synthesis*. 6 × 10⁵ HEK293T cells were transfected with 2,000 ng of (i) NL4-3 *nef* or the empty vector pCGCG, or (ii) HIV-1 NL4-3 or NL4-3 Δ*nef* proviral DNA. RNA was then isolated and purified at 6, 18, 24, and 48 h post-

Table 1. Antibody sources and conditions.

Protein	Primary antibody	Dilution	Source
ATG3	Rabbit polyclonal to ATG3	1:1000	Cell Signaling Technology, 3415S
ATG5	Rabbit polyclonal to ATG5	1:500	Cell Signaling Technology, 2630S
ATG7	Rabbit monoclonal (D12B11) to ATG7	1:500	Cell Signaling Technology, 8558S
ATG12	Rabbit monoclonal (D88H11) to ATG12	1:1000	Cell Signaling Technology, 4180S
ATG16L1	Rabbit monoclonal (D6D5) to ATG16L1	1:1000	Cell Signaling Technology, 8089S
ACTB/β-actin	Mouse monoclonal (C4) to ACTB/β-actin	1:1000	Sigma-Aldrich, MAB1501
BCL2	Mouse monoclonal (124) to BCL2	1:1000	Cell Signaling Technology, 15071S
phospho-BCL2	Rabbit monoclonal (5H2) to Phospho-BCL2/Bcl-2 (Ser70)	1:500	Cell Signaling Technology, 2827S
BECN1	Rabbit monoclonal (D40C5) to BECN1	1:1000	Cell Signaling Technology, 3495S
CD4	Rabbit polyclonal	1:500	Abcam, ab203034
Flag	Rabbit monoclonal (D6W5B)	1:400	Cell Signaling Technology, 14s793
GFP	Mouse monoclonal (4B10B2) and Rabbit monoclonal (E385) to GFP	1:1000	Sigma-Aldrich, SAB5300167
		1:1000	Abcam, ab32146
HA	Mouse monoclonal (16B12) to HA (Dylight-550 conjugated)	1:200	Abcam, ab117502
HA	Mouse monoclonal	1:1000	Covance, 901502
LC3	Rabbit polyclonal to LC3B	1:1000	Cell Signaling Technology, 2775S
MYC	Mouse monoclonal	1:1000	Abcam, ab18185
HIV Nef	Mouse monoclonal (2H12(01–007)) to HIV-1 Nef	1:1000	ThermoFisher Scientific, MA1-71505
SIV Nef	Mouse monoclonal (17.2) to SIV Nef	1:1000	NIH AIDS Reagent Program, 2659
PRKN	Mouse monoclonal (PRK8) to PRKN	1:1000	Abcam, ab77924
HIV-1 Gag p55/p24	Mouse monoclonal (183-H12-5C) to HIV p24	1:1000	NIH AIDS Reagent Program, 3537
SQSTM1/p62	Mouse monoclonal (D1Q5S) to SQSTM1/p62	1:1000	Cell Signaling Technology, 39749S
SUMO	Rabbit polyclonal to SUMO 2 + 3	1:1000	Abcam, ab139470
Ubiquitin	Rabbit monoclonal (E4I2) to Ubiquitin	1:1000	Cell Signaling Technology, 43124S
ULK1	Rabbit monoclonal (D8H5) to Ulk1	1:500	Cell Signaling Technology, 8054
UVRAG	(D2Q1Z) Rabbit monoclonal to UVRAG	1: 1000	Cell Signaling Technology, 13115S
Mouse IgG1	Goat polyclonal (HRP-conjugated)	1:2000	Pierce, 31430
Rabbit IgG1	Goat polyclonal (HRP-conjugated)	1:2000	Abcam, ab97051
Rabbit IgG	Donkey polyclonal (HRP-conjugated)	1:2000	Abcam, ab16284
Rabbit IgG1	Goat polyclonal (Alexa Fluor 633 conjugated)	1:500	ThermoFisher Scientific, A-21070

transfection, using a Qiagen RNeasy Minikit (74104) following the manufacturer's instructions. Total RNA integrity and purity was verified using a bioanalyzer (Genomics Unit, Center for Biotechnology, Texas Tech University). Only RNA samples with RIN values above 8 were used for subsequent analyses. cDNA was synthesized from 1 μg of purified RNA using an iScript cDNA synthesis kit (BioRad, 1725037). cDNA samples were subsequently used for qPCR analysis.

(ii) *qPCR.* In order to calculate *gag, LC3B*, and *ATG16L1* relative levels of expression, the SYBR green-based real-time qPCR method was used. For each reaction, SsoAdvanced universal SYBR green supermix (BioRad, 1725271) was used, together with different PrimePCR primers (BioRad, Hercules, CA) to measure RNA quality (PrimePCR RNA assay RQ1 and RQ2 primers, 10025694), genomic DNA contamination (PrimePCR gDNA, 10025352), housekeeping genes (PrimePCR human *GAPDH*) and autophagy genes (PrimePCR human *MAP1LC3B* and human *ATG16L1*). In addition, corrections for differences in transfection efficiencies were performed by quantifying *GFP* expression using the following primer pair GFP FW: 5′ CAAACTGCCTGTTCC ATGGC3′ and GFP RV: 5′ CCTTCGGGCATGAC ACTCTT3′, which gives a 120 bp amplicon. For the *gag* qPCR assays, the following primers were used Gag FW: TATCAGAAGGAGCCACCCCA and Gag RV: CCCATTCTGCAGCTTCCTCA, which generate an amplicon of 114 bp. A melting curve analysis was then performed, and mRNA levels were normalized to *GAPDH* and/or *GFP* mRNAs to obtain the relative expression levels of *gag, LC3B* and *ATG16L1* for each

time point and treatment condition. A fold change of >2.0 was considered biologically relevant.

Immunoprecipitation assays

One million HEK293T or HeLa cells were transfected with 2,000 ng of *BECN1*-Flag, *PRKN*-MYC, NL4-3 *nef*, NL4-3 *nef*-HA, human *CD4*, the empty vector pCGCG and/or the GFP-*BCL2* constructs. 48 h post-transfection, cells were washed and lysed using lysis IP buffer supplemented with phosphatase and protease inhibitor cocktails, as detailed above. The whole-cell lysates were then pre-incubated for 1 h at room temperature with Protein A or G magnetic beads (New England Biolabs, S1425S and S1430S) to remove unspecific binding proteins. Protein A or G magnetic beads were then coated with 5 μg of the antibody of interest (HIV-1 Nef, BCL2, Flag, UVRAG or BECN1; Table 1) for 1 h at room temperature. Next, cell lysates were subjected to immuno-precipitation by adding antibody-coated beads to the pre-cleared samples. The immunoprecipitation proceeded overnight at 4°C. Next, beads were washed in lysis IP buffer 4 times with the assistance of a magnet. Finally, washed beads were resuspended in 2x SDS sample buffer and the pulldown samples were analyzed by western blot. The relative binding between our proteins of interest was calculated by densitometric analyses using the Image Studio software (Li-Cor), where the positive bands were normalized to the levels of the immunoprecipitated protein.

Fluorescence microscopy

(i) LC3 and ZFYVE1 puncta. 20,000 HEK293T cells were co-transfected in sterile tissue culture-treated 8-well slides with 100 ng of EGFP-*LC3B* or GFP-*ZFYVE1* and either 100 ng of HA-

AUTOPHAGY 573

GST or NL4-3 *nef*-HA. 48 h post-transfection, cells were treated for 4 h with rapamycin at 4 µM with or without the autophagy inhibitor 3-MA at 3 mM. Cells were then washed with DPBS (ThermoFisher Scientific, 14190–144). Permeabilization and fixation of the samples were achieved by incubating the cells for 10 min in acetone-methanol (1:1) at −30°C. Next, cells were blocked for 1 h with the antibody diluent solution (2% fish skin gelatin [Sigma-Aldrich, 67765] + 0.1% Triton X-100 [Sigma-Aldrich, X100] 1x DPBS with 10% goat serum [ThermoFisher Scientific, 500062Z]) and incubated 1 more hour with the mouse monoclonal anti-HA antibody conjugated with DyLight-550 (Table 1) at a dilution of 1:200. Afterward, cells were incubated for 5 min with DAPI (1:5,000; ThermoFisher Scientific, 62248) to visualize cell nuclei. After staining, the slides were washed and mounted using the anti-quenching mounting medium (Vector Laboratories, 3304770). EGFP-LC3B-expressing cells were visualized by epifluorescence on an Olympus BX41 fluorescence microscope, using DAPI, TexasRed and GFP filter cubes and the 60x objective. Cells expressing GFP-ZFYVE1 were visualized by confocal microscopy on an Olympus FV3000 microscope using the 60x objective and the lasers 405, 488, and 561 nm in order to excite DAPI, GFP, and DyLight-550, respectively. After collection, images were processed and analyzed using the ImageJ software (National Institutes of Health) and Photoshop (Adobe), and proportional adjustments of brightness/contrast were applied.

(ii) ER-BCL2 and BECN1 colocalization. 20,000 HEK293T cells were co-transfected in sterile tissue culture-treated 8-well slides with 100 ng of *BECN1*-Flag, 100 ng of GFP-*BCL2*-Cb5 (ER-bound isoform) and either 100 ng of HA-*GST* or NL4-3 *nef*-HA. 48 h post-transfection, cells were washed with DPBS, permeabilized and fixed by incubating them for 10 min in acetone-methanol (1:1) at −30°C. Next, cells were incubated for 1 h with the antibody diluent solution (2% fish skin gelatin + 0.1% Triton X-100 1x DPBS with 10% goat serum) and 1 more hour with the following primary antibody cocktail: mouse monoclonal anti-HA primary antibody conjugated with DyLight-550 (Table 1) at a dilution of 1:200, and rabbit monoclonal anti-Flag (Table 1) at a dilution 1:400. Subsequently, cells were washed and incubated for another hour with a goat anti-rabbit IgG1 secondary antibody conjugated with an Alexa Fluor 633 fluorophore (Table 1) at a dilution 1:500. Finally, samples were incubated for 5 min with DAPI (1:5,000) to visualize cell nuclei. After staining, the slides were washed and mounted using anti-quenching mounting medium. The samples were visualized by confocal microscopy on an Olympus FV3000 instrument using the 60x objective and the lasers 405, 488, 561, and 640 nm in order to excite DAPI, GFP, DyLight-550 and Alexa Fluor 633, respectively. After collection, images were merged for the 488, 561, and 640 nm channels, processed and analyzed using ImageJ and Photoshop. Proportional adjustments of brightness/contrast were applied. Colocalization between ER-BCL2 and BECN1 was evaluated in ImageJ (JACoP plugin) by calculating Pearson's correlation coefficient.

Flow cytometry

300,000 HEK293T cells were co-transfected with 2,000 ng of EGFP-*LC3B* and 2,000 ng of either NL4-3 *nef*-HA or empty vector control. 48 h post-transfection, cells were treated with rapamycin (4 µM) and/or 3-MA (3 mM) for 4 h before collection for analysis. Cells were then washed with DPBS, trypsinized (ThermoFisher Scientific, 25200) and centrifuged at 600 x g for 5 min, followed by an additional wash of 10 min at 4°C with 0.05% saponin (Sigma-Aldrich, 47036) in DPBS. Cells were subsequently washed 2 additional times in DPBS. Finally, samples were fixed with 1% paraformaldehyde in DPBS. Cells were analyzed using an Attune instrument (ThermoFisher Scientific, Waltham, MA). Data were processed with the FlowJo software (version 10.5.3) using 50,000 events. Debris and doublets were excluded using FSC and SSC gating, and the percentage of EGFP-positive single cells was calculated for every sample and treatment condition.

Statistical analysis

All statistical calculations were performed with a two-tailed unpaired Student T test using Graph Pad Prism version 8.3.0. P values ≤ 0.05 were considered statistically significant.

Disclosure statement

No potential conflict of interest was reported by the authors.

ORCID

Konstantin Sparrer http://orcid.org/0000-0002-8682-1779

References

[1] Mizushima N. Autophagy: process and function. Genes Dev. 2007 Nov 15;21(22):2861–2873.
[2] Orvedahl A, Levine B. Viral evasion of autophagy. Autophagy. 2008 Apr;4(3):280–285.
[3] White E. The role for autophagy in cancer. J Clin Invest. 2015 Jan;125(1):42–46.
[4] Levy JMM, Towers CG, Thorburn A. Targeting autophagy in cancer. Nat Rev Cancer. 2017 Sep;17(9):528–542.
[5] Mathew R, Karantza-Wadsworth V, White E. Role of autophagy in cancer. Nat Rev Cancer. 2007 Dec;7(12):961–967.
[6] Zare-Shahabadi A, Masliah E, Johnson GV, et al. Autophagy in Alzheimer's disease. Rev Neurosci. 2015;26(4):385–395.
[7] Uddin MS, Stachowiak A, Mamun AA, et al. Autophagy and Alzheimer's Disease: from molecular mechanisms to therapeutic implications. Front Aging Neurosci. 2018;10:04.
[8] Bravo-San Pedro JM, Kroemer G, Autophagy GL. Mitophagy in Cardiovascular Disease. Circ Res. 2017 May 26;120(11):1812–1824.
[9] Lavandero S, Chiong M, Rothermel BA, et al. Autophagy in cardiovascular biology. J Clin Invest. 2015 Jan;125(1):55–64.

[10] Kang R, Zeh HJ, Lotze MT, et al. The Beclin 1 network regulates autophagy and apoptosis. Cell Death Differ. 2011 Apr;18 (4):571–580.

[11] Rubinsztein DC, Shpilka T, Elazar Z. Mechanisms of autophagosome biogenesis. Curr Biol. 2012 Jan 10;22(1):R29–34.

[12] Weidberg H, Shvets E, Elazar Z. Biogenesis and cargo selectivity of autophagosomes. Annu Rev Biochem. 2011;80:125–156.

[13] Hurley JH, Young LN. Mechanisms of autophagy initiation. Annu Rev Biochem. 2017 Jun;20(86):225–244.

[14] Matsunaga K, Saitoh T, Tabata K, et al. Two Beclin 1-binding proteins, Atg14L and Rubicon, reciprocally regulate autophagy at different stages. Nat Cell Biol. 2009 Apr;11(4):385–396.

[15] Zeng X, Overmeyer JH, Maltese WA. Functional specificity of the mammalian Beclin-Vps34 PI 3-kinase complex in macroautophagy versus endocytosis and lysosomal enzyme trafficking. J Cell Sci. 2006 Jan 15;119(Pt 2):259–270.

[16] Wang RC, Wei Y, An Z, et al. Akt-mediated regulation of autophagy and tumorigenesis through Beclin 1 phosphorylation. Science. 2012 Nov 16;338(6109):956–959.

[17] Brier LW, Ge L, Stjepanovic G, et al. Regulation of LC3 lipidation by the autophagy-specific class III phosphatidylinositol-3 kinase complex. Mol Biol Cell. 2019 Apr 15;30(9):1098–1107.

[18] Klionsky DJ, Abdelmohsen K, Abe A, et al. Guidelines for the use and interpretation of assays for monitoring autophagy (3rd edition). Autophagy. 2016;12(1):1–222.

[19] Tanida I, Waguri S. Measurement of autophagy in cells and tissues. Methods Mol Biol. 2010;648:193–214.

[20] Kirkin V, Lamark T, Johansen T, et al. NBR1 cooperates with p62 in selective autophagy of ubiquitinated targets. Autophagy. 2009 Jul;5(5):732–733.

[21] Hosokawa N, Hara T, Kaizuka T, et al. Nutrient-dependent mTORC1 association with the ULK1-Atg13-FIP200 complex required for autophagy. Mol Biol Cell. 2009 Apr;20(7):1981–1991.

[22] Kim J, Kundu M, Viollet B, et al. AMPK and mTOR regulate autophagy through direct phosphorylation of Ulk1. Nat Cell Biol. 2011 Feb;13(2):132–141.

[23] Jung CH, Jun CB, Ro SH, et al. ULK-Atg13-FIP200 complexes mediate mTOR signaling to the autophagy machinery. Mol Biol Cell. 2009 Apr;20(7):1992–2003.

[24] Di Bartolomeo S, Corazzari M, Nazio F, et al. The dynamic interaction of AMBRA1 with the dynein motor complex regulates mammalian autophagy. J Cell Biol. 2010 Oct 4;191(1):155–168.

[25] Tanida I, Sou YS, Ezaki J, et al. HsAtg4B/HsApg4B/autophagin-1 cleaves the carboxyl termini of three human Atg8 homologues and delipidates microtubule-associated protein light chain 3- and GABAA receptor-associated protein-phospholipid conjugates. J Biol Chem. 2004 Aug 27;279(35):36268–36276.

[26] Eskelinen EL. Maturation of autophagic vacuoles in mammalian cells. Autophagy. 2005 Apr;1(1):1–10.

[27] Tang SW, Ducroux A, Jeang KT, et al. Impact of cellular autophagy on viruses: insights from hepatitis B virus and human retroviruses. J Biomed Sci. 2012 Oct;30(19):92.

[28] Pugsley HR. Assessing autophagic flux by measuring LC3, p62, and LAMP1 Co-localization using multispectral imaging flow cytometry. J Vis Exp. 2017 Jul;21:125.

[29] Mizushima N, Yoshimori T. How to interpret LC3 immunoblotting. Autophagy. 2007 Nov-Dec;3(6):542–545.

[30] Schmid D, Munz C. Innate and adaptive immunity through autophagy. Immunity. 2007 Jul;27(1):11–21.

[31] Van Kaer L, Parekh VV, Postoak JL, et al. Role of autophagy in MHC class I-restricted antigen presentation. Mol Immunol. 2017 Nov 8;113:2–5.

[32] Liu Z, Xiao Y, Torresilla C, et al. Implication of DIfferent HIV-1 genes in the modulation of autophagy. Viruses. 2017 Dec 18;9 (12):389.

[33] Jordan TX, Randall G. Manipulation or capitulation: virus interactions with autophagy. Microbes Infect. 2012 Feb;14(2):126–139.

[34] Cavignac Y, Esclatine A. Herpesviruses and autophagy: catch me if you can! Viruses. 2010 Jan;2(1):314–333.

[35] Gregoire IP, Richetta C, Meyniel-Schicklin L, et al. IRGM is a common target of RNA viruses that subvert the autophagy network. PLoS Pathog. 2011 Dec;7(12):e1002422.

[36] Cheng H, Ren T, Sun SC. New insight into the oncogenic mechanism of the retroviral oncoprotein Tax. Protein Cell. 2012 Aug;3(8):581–589.

[37] Ren T, Dong W, Takahashi Y, et al. HTLV-2 Tax immortalizes human CD4+ memory T lymphocytes by oncogenic activation and dysregulation of autophagy. J Biol Chem. 2012 Oct 5;287 (41):34683–34693.

[38] Kyei GB, Dinkins C, Davis AS, et al. Autophagy pathway intersects with HIV-1 biosynthesis and regulates viral yields in macrophages. J Cell Biol. 2009 Jul 27;186(2):255–268.

[39] Denizot M, Varbanov M, Espert L, et al. HIV-1 gp41 fusogenic function triggers autophagy in uninfected cells. Autophagy. 2008 Nov;4(8):998–1008.

[40] Stremlau M, Owens CM, Perron MJ, et al. The cytoplasmic body component TRIM5alpha restricts HIV-1 infection in old world monkeys [Research Support, Non-U.S. Gov't Research Support, U.S. Gov't, Non-P.H.S. Research Support, U.S. Gov't, P.H.S.]. Nature. 2004 Feb 26;427(6977):848–853.

[41] Yap MW, Nisole S, Lynch C, et al. Trim5alpha protein restricts both HIV-1 and murine leukemia virus [Research Support, Non-U.S. Gov't]. Proc Natl Acad Sci U S A. 2004 Jul 20;101 (29):10786–10791.

[42] Stremlau M, Perron M, Welikala S, et al. Species-specific variation in the B30.2(SPRY) domain of TRIM5alpha determines the potency of human immunodeficiency virus restriction. J Virol. 2005 Mar;79(5):3139–3145.

[43] Song B, Javanbakht H, Perron M, et al. Retrovirus restriction by TRIM5alpha variants from old world and new world primates. J Virol. 2005 Apr;79(7):3930–3937.

[44] Sebastian S, Luban J. TRIM5alpha selectively binds a restriction-sensitive retroviral capsid. Retrovirology. 2005 Jun 20;2:40.

[45] Hatziioannou T, Perez-Caballero D, Yang A, et al. Retrovirus resistance factors Ref1 and Lv1 are species-specific variants of TRIM5alpha. Proc Natl Acad Sci U S A. 2004 Jul 20;101 (29):10774–10779.

[46] Mandell MA, Jain A, Arko-Mensah J, et al. TRIM proteins regulate autophagy and can target autophagic substrates by direct recognition. Dev Cell. 2014 Aug 25;30(4):394–409.

[47] Li JC, Au KY, Fang JW, et al. HIV-1 trans-activator protein dysregulates IFN-gamma signaling and contributes to the suppression of autophagy induction. AIDS. 2011 Jan 2;25(1):15–25.

[48] Campbell GR, Spector SA. Inhibition of human immunodeficiency virus type-1 through autophagy. Curr Opin Microbiol. 2013 Jun;16(3):349–354.

[49] Campbell GR, Rawat P, Bruckman RS, et al. Human immunodeficiency virus type 1 Nef inhibits autophagy through transcription factor EB sequestration. PLoS Pathog. 2015 Jun;11(6):e1005018.

[50] Chang C, Young LN, Morris KL, et al. Bidirectional control of autophagy by BECN1 BARA domain dynamics. Mol Cell. 2019 Jan 17;73(2):339–353 e6.

[51] Dinkins C, Pilli M, Kehrl JH. Roles of autophagy in HIV infection. Immunol Cell Biol. 2015 Jan;93(1):11–17.

[52] Nardacci R, Ciccosanti F, Marsella C, et al. Role of autophagy in HIV infection and pathogenesis. J Intern Med. 2017 May;281(5):422–432.

[53] Blanchet FP, Moris A, Nikolic DS, et al. Human immunodeficiency virus-1 inhibition of immunoamphisomes in dendritic cells impairs early innate and adaptive immune responses. Immunity. 2010 May 28;32(5):654–669.

[54] Espert L, Beaumelle B, Vergne I. Autophagy in mycobacterium tuberculosis and HIV infections. Front Cell Infect Microbiol. 2015;5:49.

[55] Espert L, Denizot M, Grimaldi M, et al. Autophagy is involved in T cell death after binding of HIV-1 envelope proteins to CXCR4. J Clin Invest. 2006 Aug;116(8):2161–2172.

[56] Rosa A, Chande A, Ziglio S, et al. HIV-1 Nef promotes infection by excluding SERINC5 from virion incorporation. Nature. 2015 Oct 8;526(7572):212–217.

[57] Usami Y, Wu Y, Gottlinger HG. SERINC3 and SERINC5 restrict HIV-1 infectivity and are counteracted by Nef. Nature. 2015 Oct 8;526(7572):218–223.

[58] Williams M, Roeth JF, Kasper MR, et al. Direct binding of human immunodeficiency virus type 1 Nef to the major histocompatibility complex class I (MHC-I) cytoplasmic tail disrupts MHC-I trafficking. J Virol. 2002;76:12173–12184.

[59] Roeth JF, Williams M, Kasper MR, et al. HIV-1 Nef disrupts MHC-I trafficking by recruiting AP-1 to the MHC-I cytoplasmic tail [Research Support, Non-U.S. Gov't Research Support, U.S. Gov't, P.H.S.]. J Cell Biol. 2004 Dec 6;167(5):903–913.

[60] Mangasarian A, Piguet V, Wang J-K, et al. Nef-induced CD4 and major histocompatibility complex class I (MHC-I) down-regulation are governed by distinct determinants: N-terminal alpha helix and proline repeat of Nef selectively regulate MHC-I trafficking. J Virol. 1999;73:1964–1973.

[61] Fackler OT, Moris A, Tibroni N, et al. Functional characterization of HIV-1 Nef mutants in the context of viral infection [Research Support, Non-U.S. Gov't]. Virology. 2006 Aug 1;351(2):322–339.

[62] Jia X, Singh R, Homann S, et al. Structural basis of evasion of cellular adaptive immunity by HIV-1 Nef [Research Support, N.I.H., Extramural Research Support, Non-U.S. Gov't]. Nat Struct Mol Biol. 2012 Jul;19(7):701–706.

[63] Swigut T, Shody N, Skowronski J. Mechanism for down-regulation of CD28 by Nef. Embo J. 2001;20:1593–1604.

[64] Stove V, Van de Walle I, Naessens E, et al. Human immunodeficiency virus Nef induces rapid internalization of the T-cell coreceptor CD8alphabeta [Research Support, Non-U.S. Gov't]. J Virol. 2005 Sep;79(17):11422–11433.

[65] Munch J, Rajan D, Schindler M, et al. Nef-mediated enhancement of virion infectivity and stimulation of viral replication are fundamental properties of primate lentiviruses. J Virol. 2007 Dec;81 (24):13852–13864.

[66] Sagnier S, Daussy CF, Borel S, et al. Autophagy restricts HIV-1 infection by selectively degrading Tat in CD4+ T lymphocytes. J Virol. 2015 Jan;89(1):615–625.

[67] Mandell MA, Kimura T, Jain A, et al. TRIM proteins regulate autophagy: TRIM5 is a selective autophagy receptor mediating HIV-1 restriction. Autophagy. 2014;10(12):2387–2388.

[68] Borel S, Robert-Hebmann V, Alfaisal J, et al. HIV-1 viral infectivity factor interacts with microtubule-associated protein light chain 3 and inhibits autophagy. AIDS. 2015 Jan 28;29(3):275–286.

[69] Mizushima N. Methods for monitoring autophagy. Int J Biochem Cell Biol. 2004 Dec;36(12):2491–2502.

[70] Man N, Chen Y, Zheng F, et al. Induction of genuine autophagy by cationic lipids in mammalian cells. Autophagy. 2010 May;6 (4):449–454.

[71] Schmid D, Pypaert M, Munz C. Antigen-loading compartments for major histocompatibility complex class II molecules continuously receive input from autophagosomes. Immunity. 2007 Jan;26(1):79–92.

[72] Sakaki K, Kaufman RJ. Regulation of ER stress-induced macroautophagy by protein kinase C. Autophagy. 2008 Aug;4(6):841–843.

[73] Sakaki K, Wu J, Kaufman RJ. Protein kinase Ctheta is required for autophagy in response to stress in the endoplasmic reticulum. J Biol Chem. 2008 May 30;283(22):15370–15380.

[74] Tan SH, Shui G, Zhou J, et al. Induction of autophagy by palmitic acid via protein kinase C-mediated signaling pathway independent of mTOR (mammalian target of rapamycin). J Biol Chem. 2012 Apr 27;287(18):14364–14376.

[75] Botbol Y, Patel B, Macian F. Common gamma-chain cytokine signaling is required for macroautophagy induction during CD4 + T-cell activation. Autophagy. 2015;11(10):1864–1877.

[76] Hubbard VM, Valdor R, Patel B, et al. Macroautophagy regulates energy metabolism during effector T cell activation. J Immunol. 2010 Dec 15;185(12):7349–7357.

[77] McFarlane S, Aitken J, Sutherland JS, et al. Early induction of autophagy in human fibroblasts after infection with human cytomegalovirus or herpes simplex virus 1. J Virol. 2011 May;85 (9):4212–4221.

[78] Rasmussen SB, Horan KA, Holm CK, et al. Activation of autophagy by alpha-herpesviruses in myeloid cells is mediated by cytoplasmic viral DNA through a mechanism dependent on stimulator of IFN genes. J Immunol. 2011 Nov 15;187(10):5268–5276.

[79] Konno H, Konno K, Barber GN. Cyclic dinucleotides trigger ULK1 (ATG1) phosphorylation of STING to prevent sustained innate immune signaling. Cell. 2013 Oct 24;155(3): 688–698.

[80] Jia B, Serra-Moreno R, Neidermyer W, et al. Species-specific activity of SIV Nef and HIV-1 Vpu in overcoming restriction by tetherin/BST2. PLoS Pathog. 2009 May;5(5):e1000429.

[81] Serra-Moreno R, Zimmermann K, Stern LJ, et al. Tetherin/BST-2 antagonism by Nef depends on a direct physical interaction between Nef and tetherin, and on clathrin-mediated endocytosis. PLoS Pathog. 2013 Jul;9(7):e1003487.

[82] Serra-Moreno R, Jia B, Breed M, et al. Compensatory changes in the cytoplasmic tail of gp41 confer resistance to tetherin/BST-2 in a pathogenic nef-deleted SIV. Cell Host Microbe. 2011 Jan 20;9 (1):46–57.

[83] Nityanandam R, Serra-Moreno R, Krausslich H-G. BCA2/ Rabring7 targets HIV-1 Gag for lysosomal degradation in a tetherin-independent manner [Research Support, N.I.H., Extramural Research Support, Non-U.S. Gov't]. PLoS Pathog. 2014 May;10(5):e1004151.

[84] Rubinsztein DC, Codogno P, Levine B. Autophagy modulation as a potential therapeutic target for diverse diseases. Nat Rev Drug Discov. 2012 Sep;11(9):709–730.

[85] Shoji-Kawata S, Sumpter R, Leveno M, et al. Identification of a candidate therapeutic autophagy-inducing peptide. Nature. 2013 Feb 14;494(7436):201–206.

[86] Jung CH, Ro SH, Cao J, et al. mTOR regulation of autophagy. FEBS Lett. 2010 Apr 2;584(7):1287–1295.

[87] Jewell JL, Russell RC, Guan KL. Amino acid signalling upstream of mTOR. Nat Rev Mol Cell Biol. 2013 Mar;14(3):133–139.

[88] Wong PM, Feng Y, Wang J, et al. Regulation of autophagy by coordinated action of mTORC1 and protein phosphatase 2A. Nat Commun. 2015 Aug 27;6:8048.

[89] Fullgrabe J, Ghislat G, Cho DH, et al. Transcriptional regulation of mammalian autophagy at a glance. J Cell Sci. 2016 Aug 15;129 (16):3059–3066.

[90] Napolitano G, Ballabio A. TFEB at a glance. J Cell Sci. 2016 Jul 1;129(13):2475–2481.

[91] Settembre C, Ballabio A. TFEB regulates autophagy: an integrated coordination of cellular degradation and recycling processes. Autophagy. 2011 Nov;7(11):1379–1381.

[92] Axe EL, Walker SA, Manifava M, et al. Autophagosome formation from membrane compartments enriched in phosphatidylinositol 3-phosphate and dynamically connected to the endoplasmic reticulum. J Cell Biol. 2008 Aug 25;182(4):685–701.

[93] Chang NC, Nguyen M, Germain M, et al. Antagonism of Beclin 1-dependent autophagy by BCL-2 at the endoplasmic reticulum requires NAF-1. Embo J. 2010 Feb 3;29(3):606–618.

[94] Marquez RT, Xu L. Bcl-2:Beclin 1 complex: multiple, mechanisms regulating autophagy/apoptosis toggle switch. Am J Cancer Res. 2012;2(2):214–221.

[95] Pattingre S, Tassa A, Qu X, et al. Bcl-2 antiapoptotic proteins inhibit Beclin 1-dependent autophagy. Cell. 2005 Sep 23;122(6):927–939.

[96] Kihara A, Kabeya Y, Ohsumi Y, et al. Beclin-phosphatidylinositol 3-kinase complex functions at the trans-Golgi network. EMBO Rep. 2001 Apr;2(4):330–335.

[97] Menon MB, Dhamija S. Beclin 1 phosphorylation - at the center of autophagy regulation. Front Cell Dev Biol. 2018;6:137.

[98] Tang D, Kang R, Livesey KM, et al. Endogenous HMGB1 regulates autophagy. J Cell Biol. 2010 Sep 6;190(5):881–892.

[99] Song X, Zhu S, Chen P, et al. AMPK-mediated BECN1 phosphorylation promotes ferroptosis by directly blocking system Xc(-) activity. Curr Biol. 2018 Aug 6;28(15):2388–2399 e5.

[100] Chen D, Gao F, Li B, et al. Parkin mono-ubiquitinates Bcl-2 and regulates autophagy. J Biol Chem. 2010 Dec 3;285(49):38214–38223.

[101] Liang XH, Kleeman LK, Jiang HH, et al. Protection against fatal Sindbis virus encephalitis by beclin, a novel Bcl-2-interacting protein. J Virol. 1998 Nov;72(11):8586–8596.

[102] Carroll RG, Hollville E, Martin SJ. Parkin sensitizes toward apoptosis induced by mitochondrial depolarization through promoting degradation of Mcl-1. Cell Rep. 2014 Nov 20;9(4):1538–1553.

[103] Hollville E, Carroll RG, Cullen SP, et al. Bcl-2 family proteins participate in mitochondrial quality control by regulating Parkin/PINK1-dependent mitophagy. Mol Cell. 2014 Aug 7;55(3):451–466.

[104] Lutz AK, Exner N, Fett ME, et al. Loss of parkin or PINK1 function increases Drp1-dependent mitochondrial fragmentation. J Biol Chem. 2009 Aug 21;284(34):22938–22951.

[105] Lama J, Mangasarian A, Trono D. Cell-surface expression of CD4 reduces HIV-1 infectivity by blocking Env incorporation in a Nef- and Vpu-inhibitable manner. Curr Biol. 1999 Jun 17;9(12):622–631.

[106] Rossi F, Gallina A, Milanesi G. Nef-CD4 physical interaction sensed with the yeast two-hybrid system. Virology. 1996 Mar 1;217(1):397–403.

[107] Harris MP, Neil JC. Myristoylation-dependent binding of HIV-1 Nef to CD4. J Mol Biol. 1994 Aug 12;241(2):136–142.

[108] Grzesiek S, Stahl SJ, Wingfield PT, et al. The CD4 determinant for down-regulation by HIV-1 Nef directly binds to Nef. Mapping of the Nef binding surface by NMR. Biochemistry. 1996 Aug 13;35(32):10256–10261.

[109] Preusser A, Briese L, Baur AS, et al. Direct in vitro binding of full-length human immunodeficiency virus type 1 Nef protein to CD4 cytoplasmic domain. J Virol. 2001 Apr;75(8):3960–3964.

[110] Bentham M, Mazaleyrat S, Harris M. The di-leucine motif in the cytoplasmic tail of CD4 is not required for binding to human immunodeficiency virus type 1 Nef, but is critical for CD4 down-modulation. J Gen Virol. 2003 Oct;84(Pt 10):2705–2713.

[111] Jin YJ, Zhang X, Boursiquot JG, et al. CD4 phosphorylation partially reverses Nef down-regulation of CD4. J Immunol. 2004 Nov 1;173(9):5495–5500.

[112] Cluet D, Bertsch C, Beyer C, et al. Detection of human immunodeficiency virus type 1 Nef and CD4 physical interaction in living human cells by using bioluminescence resonance energy transfer. J Virol. 2005 Jul;79(13):8629–8636.

[113] Thomenius MJ, Distelhorst CW. Bcl-2 on the endoplasmic reticulum: protecting the mitochondria from a distance. J Cell Sci. 2003 Nov 15;116(Pt 22):4493–4499.

[114] Wang NS, Unkila MT, Reineks EZ, et al. Transient expression of wild-type or mitochondrially targeted Bcl-2 induces apoptosis, whereas transient expression of endoplasmic reticulum-targeted Bcl-2 is protective against Bax-induced cell death. J Biol Chem. 2001 Nov 23;276(47):44117–44128.

[115] Lee ST, Hoeflich KP, Wasfy GW, et al. Bcl-2 targeted to the endoplasmic reticulum can inhibit apoptosis induced by Myc but not etoposide in Rat-1 fibroblasts. Oncogene. 1999 Jun 10;18(23):3520–3528.

[116] Oberstein A, Jeffrey PD, Shi Y. Crystal structure of the Bcl-XL-Beclin 1 peptide complex: beclin 1 is a novel BH3-only protein. J Biol Chem. 2007 Apr 27;282(17):13123–13132.

[117] Akao Y, Otsuki Y, Kataoka S, et al. Multiple subcellular localization of bcl-2: detection in nuclear outer membrane, endoplasmic reticulum membrane, and mitochondrial membranes. Cancer Res. 1994 May 1;54(9):2468–2471.

[118] Krajewski S, Tanaka S, Takayama S, et al. Investigation of the subcellular distribution of the bcl-2 oncoprotein: residence in the nuclear envelope, endoplasmic reticulum, and outer mitochondrial membranes. Cancer Res. 1993 Oct 1;53(19):4701–4714.

[119] Janiak F, Leber B, Andrews DW. Assembly of Bcl-2 into microsomal and outer mitochondrial membranes. J Biol Chem. 1994 Apr 1;269(13):9842–9849.

[120] Narendra D, Tanaka A, Suen DF, et al. Parkin is recruited selectively to impaired mitochondria and promotes their autophagy. J Cell Biol. 2008 Dec 1;183(5):795–803.

[121] Itakura E, Kishi C, Inoue K, et al. Beclin 1 forms two distinct phosphatidylinositol 3-kinase complexes with mammalian Atg14 and UVRAG. Mol Biol Cell. 2008 Dec;19(12):5360–5372.

[122] Itakura E, Mizushima N. Atg14 and UVRAG: mutually exclusive subunits of mammalian Beclin 1-PI3K complexes. Autophagy. 2009 May;5(4):534–536.

[123] Kirchhoff F, Schindler M, Specht A, et al. Role of Nef in primate lentiviral immunopathogenesis. Cell Mol Life Sci. 2008 Sep;65(17):2621–2636.

[124] Schmokel J, Li H, Bailes E, et al. Conservation of Nef function across highly diverse lineages of SIVsmm. Retrovirology. 2009 Apr;9(6):36.

[125] Serra-Moreno R, Evans DT. Adaptation of human and simian immunodeficiency viruses for resistance to tetherin/BST-2. Curr HIV Res. 2012 Jun 1;10(4):277–282.

[126] Neil SJ, Zang T, Bieniasz PD. Tetherin inhibits retrovirus release and is antagonized by HIV-1 Vpu. Nature. 2008 Jan 24;451 (7177):425–430.

[127] Van Damme N, Goff D, Katsura C, et al. The interferon-induced protein BST-2 restricts HIV-1 release and is downregulated from the cell surface by the viral Vpu protein. Cell Host Microbe. 2008 Apr 17;3(4):245–252.

[128] Zhang F, Wilson SJ, Landford WC, et al. Nef proteins from simian immunodeficiency viruses are tetherin antagonists. Cell Host Microbe. 2009 Jul 23;6(1):54–67.

[129] Le Tortorec A, Neil SJ. Antagonism and intracellular sequestration of human tetherin by the HIV-2 envelope glycoprotein. J Virol. 2009 Sep 9;83:11966–11978.

[130] Sauter D, Schindler M, Specht A, et al. Tetherin-driven adaptation of Vpu and Nef function and the evolution of pandemic and nonpandemic HIV-1 strains. Cell Host Microbe. 2009 Nov 19;6(5):409–421.

[131] Sauter D, Kirchhoff F. Tetherin antagonism by primate lentiviral nef proteins. Curr HIV Res. 2011 Oct 1;9(7):514–523.

[132] Alexander L, Illyinskii PO, Lang SM, et al. Determinants of increased replicative capacity of serially passaged simian immunodeficiency virus with nef deleted in rhesus monkeys. J Virol. 2003;77:6823–6835.

[133] Parzych KR, Klionsky DJ. An overview of autophagy: morphology, mechanism, and regulation. Antioxid Redox Signal. 2014 Jan 20;20(3):460–473.

[134] Codogno P, Mehrpour M, Proikas-Cezanne T. Canonical and non-canonical autophagy: variations on a common theme of self-eating? Nat Rev Mol Cell Biol. 2012 Jan;13(1):7–12.

[135] Dowaidar M, Gestin M, Cerrato CP, et al. Role of autophagy in cell-penetrating peptide transfection model. Sci Rep. 2017 Oct 3;7(1):12635.

[136] Barth S, Glick D, Macleod KF. Autophagy: assays and artifacts. J Pathol. 2010 Jun;221(2):117–124.

[137] Chang C, Young LN, Hurley JH. The BARA necessities of PtdIns 3-kinase activation in autophagy. Autophagy. 2019 Jun;15(6):1122–1123.

[138] Decuypere JP, Parys JB, Bultynck G. Regulation of the autophagic bcl-2/beclin 1 interaction. Cells. 2012 Jul 6;1(3):284–312.

[139] DeGottardi MQ, Specht A, Metcalf B, et al. Selective downregulation of rhesus macaque and sooty mangabey major histocompatibility complex class I molecules by nef alleles of simian immunodeficiency virus and human immunodeficiency virus type 2. J Virol. 2008;82:3139–3146.

[140] Adachi A, Gendelman HE, Koenig S, et al. Production of acquired immunodeficiency virus syndrome-associated retrovirus in human and nonhuman cells transfected with an infectious molecular clone. J Virol. 1986;59:284–291.

[141] Strebel K, Klimkait T, Martin MA. A novel gene of HIV-1, vpu, and its 16-kilodalton product. Science. 1988;241:1221–1223.

[142] Zhang H, Zhou Y, Alcock C, et al. Novel single-cell-level phenotypic assay for residual drug susceptibility and reduced replication capacity of drug-resistant human immunodeficiency virus type 1. J Virol. 2004 Feb;78(4):1718–1729.

[143] Schwartz O, Marechal V, Danos O, et al. Human immunodeficiency virus type 1 Nef increases the efficiency of reverse transcription in the infected cell. J Virol. 1995 Jul;69 (7):4053–4059.

[144] Colomer-Lluch M, Serra-Moreno R. BCA2/Rabring7 interferes with hiv-1 proviral transcription by enhancing the SUMOylation of IkappaBalpha. J Virol. 2017 Apr 15;91:8.

[145] Kestler HW, Ringler DJ, Mori K, et al. Importance of the nef gene for maintenance of high virus loads and for the development of AIDS. Cell. 1991;65:651–662.

[146] Regier DA, Desrosiers RC. The complete nucleotide sequence of a pathogenic molecular clone of simian immunodeficiency virus. AIDS Res Hum Retroviruses. 1990;6:1221–1231.

[147] Heigele A, Kmiec D, Regensburger K, et al. The potency of Nef-Mediated SERINC5 antagonism correlates with the prevalence of primate lentiviruses in the wild. Cell Host Microbe. 2016 Sep 14;20(3):381–391.

[148] Arias JF, Colomer-Lluch M, von Bredow B, et al. Tetherin antagonism by HIV-1 Group M Nef proteins. J Virol. 2016 Sep 21;90:10701–10714.